Experimental and numerical modelling of hygrothermal transfer: Application on building energy performance

Fouad Boukhelf, Abdelkrim Trabelsi, Rafik Belarbi, Mohamed Bachir Bouiadjra

Experimental and numerical modelling of hygrothermal transfer: Application on building energy performance

Fouad BOUKHELF[a,b,c,d*], Abdelkrim TRABELSI[e], Rafik BELARBI[b,d], Mohamed BACHIR BOUIADJRA[c]

[a] COMUE Normandie Université – Laboratoire ESITC, 1 Rue Pierre et Marie Curie, 14610, Epron, France.

[b] LaSIE, UMR CNRS 7356, La Rochelle University, Av Michel Crépeau, 17042 La Rochelle Cedex 1, France.

[c] Laboratoire des Structures et Matériaux Avancés dans le Génie Civil et Travaux Publics, University of Sidi Bel Abbes, Faculty of Technology, Civil Engineering Department, Algeria.

[d] 4evLab, LaSIE, CNRS, EDF R&D, La Rochelle University, Avenue Michel Crépeau 17042, La Rochelle Cedex1, France

[e] Univ Lyon, CNRS, INSA-Lyon, Université Claude Bernard Lyon 1, CETHIL UMR5008, F-69621 Villeurbanne, France.

[*]Corresponding author: COMUE Normandie Université – Laboratoire ESITC, 1 Rue Pierre et Marie Curie, 14610, Epron, France. Tel: +33 (0)2 31 46 23 02. Email: fouad.boukhelf@esitc-caen.fr

Abstract

This work deals with the hygrothermal behavior of building envelope wall composed of an eco-concrete made of glass powder. The material was chosen in order to satisfy the RE2020 requirements regarding the carbon footprint reduction of building materials. The wall is tested and subjected to wetting/drying cycles by T/RH variations with/without solar radiations and rainfall. The last two climatic conditions are real and rarely taken into account in the study of hygrothermal behavior. Therefore, an experimental set-up was designed and a numerical model was proposed. The numerical and experimental results were compared for the both tests. The results obtained highlighted the ability of the numerical model to reproduce the hygrothermal behavior of the wall. For Test 1, the RMSE value is about 0.24 °C, 4.78 % and 2.28 W.m^{-2} for T, RH and thermal flux, respectively. Whereas, it is about 0.23 °C, 3.47 % and 7.79 W.m^{-2} for Test 2. The impact of rainfall is 3.33 time more than the test without rain for a material with porosity about 14.18%. As for drying, the solar radiations has an important intensity of about 820 W.m^{-2} and induces a significant heat flux at the external border.

Keywords: Hygrothermal transfer; Solar radiation; Rainfall; Experimental bench; Eco-concrete; Chemical analysis.

Nomenclature

Term	Signification	Unit
C_m	Hydric capacity	(-)
C_p	Heat capacity	$J.K^{-1}.kg^{-1}$
$C_{p\ dry}$	Heat capacity of dry material	$J.K^{-1}.kg^{-1}$
$C_{p\ water}$	Heat capacity of water	$J.K^{-1}.kg^{-1}$
D_w	Hydric diffusivity	$m^2.s^{-1}$
h_l	Mass enthalpy of liquid water	$J.kg^{-1}$
h_v	Mass enthalpy of vapor water	$J.kg^{-1}$
J_l	Liquid flow density	$kg.m^{-2}.s^{-1}$
J_q	Heat flux density	$W.m^{-2}$
J_v	Vapor flow density	$kg.m^{-2}.s^{-1}$
k_l	water liquid permeability	$kg.Pa^{-1}.m^{-1}.s^{-1}$
K_{PP}	Moisture transfer coefficient	$kg.Pa^{-1}.m^{-1}.s^{-1}$
K_{PT}	Moisture transfer coefficient associated with heat transfer	$J.s.m^{-3}.K^{-1}$
K_{TP}	Heat transfer coefficient associated with moisture transfer	$W.kg^{-1}$
K_{TT}	Heat transfer coefficient	$W.m^{-1}.K^{-1}$
λ_{dry}	Thermal conductivity of dry material	$W.m^{-1}.K^{-1}$
λ_{water}	Thermal conductivity of water	$W.m^{-1}.K^{-1}$
ln	Logarithm	
L_v	Latent heat of vaporization	$J.kg^{-1}$
LWL	Long wavelength radiation	$W.m^{-2}$
M	Molar mass	$kg.mol^{-1}$
ME	Mean error	
P_c	capillary pressure	Pa
P_v	Vapor pression	Pa
$P_{v,sat}$	Satu ation vapor pressure	Pa
R	Perfect gas constant	$J.mol^{-1}.K^{-1}$
R^2	R squared	(-)
RH	Relative humidity	(%)
$RMSE$	Root Mean Square Error	
σ	Ratio of vapor flow to hydric flow	(-)
SWL	Short wavelength radiation	$W.m^{-2}$
T	Temperature	K
t	Time	s
w	Water cont nt	$kg.m^{-3}$
u	Water content	$kg.kg^{-1}$
δ_p	Water vapor permeability	$kg.Pa^{-1}.m^{-1}.s^{-1}$
λ	Thermal conductivity	$W.m^{-1}.K^{-1}$
ρ_l	density of water in liquid state	$kg.m^{-3}$
ρ_s	dry density of material	$kg.m^{-3}$
S	Sensitivity	%

Y	Model's variable (T or Pv)
p	Model's parameter
δ	Variation range

Highlights

- Heat and mass transfer characteristics are studied experimentally and numerically.
- Real climatic conditions as solar radiation and rainfall are selected for the study of building envelope elements at wall scale.
- An eco-concrete wall with a replacement of cement by 20% of glass powder is tested.
- A new experimental set-up was designed which can generate solar radiations and rainfall.
- Sensitivity analysis of heat and moisture transfer model was performed.

1 Introduction

1.1 Background

The environmental impact of buildings makes the energy efficiency of buildings a crucial challenge for designers and engineers in order to minimize their energy bill and CO_2 emissions. This requires an accurate prediction of the thermal losses of building envelopes. Moreover, moisture is an important factor since it has an impact on the performance through latent heat exchange, and is strongly coupled with thermal transfer. In this context, several models have been proposed in the literature to predict the physical phenomena of hygrothermal transfer in porous materials. Among others, the building envelope is exposed to the various dynamic influences and conditions of the external environment (radiation, rain, temperature, wind...) as well as those of the internal environment (heating, ventilation, different sources of heat and humidity...). Under all these conditions, the envelope is subject to complex heat and mass transfer phenomena. The Executive Committee of the International Agency for Energy in Buildings and Community Systems has initiated in 2003 the Annex 41 [1] "Whole Building Heat, Air, and Moisture Response". In this annex, experimental campaigns of coupled heat, mass and air transfers in the building envelope were conducted in order to compare the results with those of the predictions of twelve numerical tools for the simulation of transfers at the building envelope scale. The main objective was to fortify and verify the reliability of these prediction tools by comparing them with experimental results [2,3]. The experiments were carried out in scale 1 test cells. The principle of each experiment was to measure the influence of the materials on the hygroscopic buffering capacity of the interior facings of each cell. The results obtained showed a very good correlation between the measured and calculated relative interior humidities in the case of a non-hygroscopic interior facing. In contrast, the 12 models tested had more difficulty simulating the indoor relative humidity in the case of a hygroscopic interior facing [4].

Numerical modeling and simulation is a useful method for studying or designing building envelopes. The modeling of coupled heat and mass transfers in envelopes is based on several phenomenological

approaches which differ principally in the transfer potentials used. For heat transfer, temperature is referred to as a conventional transfer potential. For humidity transfer, on the other hand, there is no unanimity. There are several models with different moisture transfer driving forces as water content [5], vapor pressure [6,7], vapor content [8,9] and relative humidity [10,11].

Luikov [12] was one of the pioneers in proposing a model taking into account heat and mass coupling transfers in porous materials. This model considers that water vapor diffusion depends on the mass water content gradient (u) and temperature (T) on the one hand, and on the total pressure gradient (P) inside the porous material on the other hand [13]. However, it suggests separating the vapor and liquid flows. This model has been refined in many research studies [14,15]. The major difficulty of this model lies in the determination of the model parameters by separating the transfer of the liquid and vapor phase and in the determination of the thermal gradient coefficient. An experimental bench has been proposed for this purpose in the research studies by Trabelsi et al. [13] to evaluate this coefficient.

Accordingly, the IEA-Annex 24 [16] was reported the modeling of six tools handling heat, air and moisture. In the work of Grunewald et al [17], the convective flows as heat and moisture vectors in porous materials to diffusion were added explicitly. Janssens et al [18] proposed a two dimensional model that predicted the heat, air, moisture response of building roofs. Ten Wolde et al [19] and Hens et al [20] enhanced the diffusion method by adding the air coupled to enthalpy and vapor transport.

Experimental study of the hygrothermal behavior of building walls at the intermediate scale is the subject of several research works in the literature, which deal with comparison of the results predicted by mathematical models and experimental results. Rahim et al. [21] developed an experimental set-up presented in a climatic chamber with temperature and humidity regulated to simulate the external environment. In addition, one of its sides was closed by the wall under study. Humidity and temperature sensors were incorporated in the wall, making it possible to monitor the evolution of the temperature and humidity. Analysis of the hygrothermal behavior of a 1:1 scale wall subjected to static and dynamic environmental conditions in terms of temperature and humidity was undertaken. The numerical simulation showed the need to take into account the heterogeneity of the material, the influence of temperature as well as the hysteresis phenomenon on the sorption curves on mass transfer. In addition, Moradias et al. [22] investigated experimentally the hygrothermal behavior of renovated stone masonry walls of old buildings, using a climate chamber in which temperature and humidity variations that occur in a stone masonry wall were measured. The results obtained in the laboratory were compared with the analytical results of the Glaser method obtained using dedicated software for the evaluation of the probability of occurrence of internal condensation in walls. Besides, Ferroukhi et al. [23] developed an experimental set-up consisting of two chambers with controlled humidity and temperature simulating the outdoor climate and the building atmosphere. The climate of the two

chambers was provided by temperature and humidity generators. Sensors were installed at different positions in the two chambers and in the studied wall.

Slimani et al. [8] also presented an experimental bench with two humidity and temperature controlled chambers. Extensive instrumentation was installed for the measurement of water and heat flows, as well as the temperature and humidity at the wall profile, and in both environments the measurement of air speed and the pressure difference between the two environments. The objective of this set-up was to study and analyze the hygrothermal behavior in the walls of the building envelope, to validate HAM models, or to characterize, at the scale of the wall, the transfer properties.

More recently, Tejeda et al. [24] designed a hot box in order to evaluate the hygrothermal behavior of the sample. This latter was calibrated using a reference sample of extruded polystyrene plate to quantify the heat gains through its envelope. The solid block wall sample was evaluated in three configurations (simple wall, wall with a mortar coat and a wall with a mortar coat on both sides). Simultaneously, three empirical models were obtained to determine the global heat transfer coefficient related with temperature and vapour pressure. In addition, Congedo et al. [25] highlighted the study of rising damp which is considered as one of the most widespread and damaging deterioration processes for buildings and architectural and cultural heritage. In this work, the dynamic assessment of rising damp is established on two types of building stones widely used in Italy, namely the stone of Lecce and Carparopar a following of the weight of the wet samples and the height of the humidity rise. At the end of the experimental campaign, the behavior of the water romentation was predicted using the theoretical model. Also, Hamdaoui et al. [26] has established a comprehensive state of the art of physical and data-driven models of building hygrothermal behavior. This study highlights the need for a recognized method for hygrothermal simulations of hygroscopic envelopes. It provides a better understanding of hygrothermal simulation, which helps in selecting the most appropriate tool or model.

To our knowledge , rain is rarely used in hygrothermal transfers modeling. In the studies of Kunzel [27] and Rouchier et al. [28], rain infiltration was added through a liquid water flow. Morever, in the work of Janssen [29] they also modeled driving rain on a building wall. The mass balance on the external surface is constituted by rain water and vapor exchange. The boundary conditions used are flow conditions. As long as the exposed external facade does not reach capillary saturation, there is moisture exchange with the atmosphere gas, including rain driven with wind and water vapor.

Wind-driven rain can be retained as a function of the coefficient of interaction between the wind, rain and wall, and this coefficient depends on the wind speed and its direction from the wall with respect to North, the amount of horizontal rain, and the orientation of the wall with respect to North [30]. In work carried out by Ihara et al., [31], an experimental bench (Atlas SC 600 MHG Solar Simulator, Vötsch Industrietechnik GmbH, Germany) simulating solar radiation and moisture variation is used

with the aim of investigating the application of aerogel in the building and construction sector and thus its durability. This work focused on the aging effect of aerogel granules, with emphasis on two aging factors, humidity and solar radiation. In addition, previous numerical studies also consider runoff from exterior building facades [32,33], furthermore ASHRAE Project 1235 confirmed that wet capillary exterior finishes, such as brick veneers, induce solar-induced vapor flow with moisture deposition in the interior layers of thermal insulation [34].

Generally, the construction materials are characterized according to recommendations relating to standards at the material scale. These properties, which also have input parameters to build numerical simulation models, are nevertheless insufficient to take into account the hygrothermal behavior of a 1:1 scale wall of a building because of its heterogeneity and the influence of variable environmental conditions. Experimental validation is necessary at an intermediate scale to provide more representative information with better control of boundary conditions.

Solar radiation is in the short wavelength between 300 and 3,000 nm. The solar radiation flux at the external surface is given in several research works [35–37]. It is the combination of the absorbed short wavelength solar energy and the long wavelength radiation exchanged with the surface, sky and multiple adjacent walls and surfaces.

Currently, there is little work dealing with experimental work of mass and heat transfer taking into account solar radiation and rainfall. The interest in taking these parameters into account is to qualify the facades and predict the service life of constructions [38]. Recently, researchers have studied the effect of rain or solar radiation at the building level to qualify the quality of façade cladding based on fibrous materials [39], by using Wufi ® to evaluate the influence of the placement of interior or exterior thermal insulation layers on the hygrothermal behavior of the envelope element [40] and experimental study to evaluate the hygrothermal performance assessment of wood frame wall systems [41]. These studies were carried out on site under real climatic conditions, which had the advantage of studying the envelope in operation. Nevertheless, under these conditions the analysis of the transfer mechanisms becomes difficult and it is mainly for this reason that the development of an experimental bench under controlled laboratory conditions was chosen. This allows, among other reasons, the simulation of loading sequences, which facilitates the analysis of hygrothermal transfer mechanisms. The studies of Rahim et al. [21], Ferroukhi et al. [23], Slimani et al. [8] and Rafidiarison et al. [42] have developed experimental benches under controlled laboratory conditions but these do not allow for the effects of solar radiation/rainfall to be considered.

1.2. Aim of the study

Following the literature state of art existing, the taking into account of solar radiation and a rainfall in the hygrothermal behavior study is little mentioned and needs further studies [43]. For this purpose,

the following methodology was established and summarized in Fig. 1. Firstly, a mathematical model fot the prediction of the hygrothermal transfer was proposed and a new set-up was designed. This latter is composed of two chambers controlled in solar radiation, temperature and water spray, the first simulating the external environment and the second simulating the habitable environment. The advantages of this set-up are that it takes into account the different climatic conditions, in particular solar radiation, rainfall and changes in temperature and humidity.

Secondary, with the goal to address the requirements of the RE2020 environmental regulation [44] in terms of greenhouse gas emission reduction and sustainable construction in the building sector, we have been interested to the use of solid waste glass as partial replacement of cement. To be precise, the glass powder incorporated in concrete is both beneficial to environmental protection and economic development. In this work, an investigation on eco-concretes is established on the wall scale, evaluating the hygrothermal behavior of this material for an application in building envelope elements. Physical principals has been confirmed by the experimental bench implemented.

Subsequently, two scenarios of hygrothermal conditions were programed in order to validate the prediction model. The first consists of varying the temperature sinusoidally over a period of 24 hours a day for 7 days without solar radiation or rain. The second retains the same temperature variation but is accompanied by solar radiation and rainfall applied alternately for periods of 1 hour intervals. Morever, the chemical resistance is established through the chemical analysis of the water used to simulate rainfall before and after the rain sequences. The quantities of released chemical species from the wall are evaluated which will inform us about the sustainability of the eco-concrete regarding chemical degradation. This first step allowed us to plan a further study in which the chemical composition through the thickness of the wall will be studied using destructive methods.

Finally, a sensitivity analysis is performed on the developed hygrothermal model, while it is applied to a glass powder-based eco-concrete. In this part, the influence of a wide range of parameters of order 20% on the specific heat, thermal conductivity, density, water vapor/liquid permeability and sorption isotherm is explored. A local sensitivity analysis method is used to separately capture the influence of each parameter on the model result.

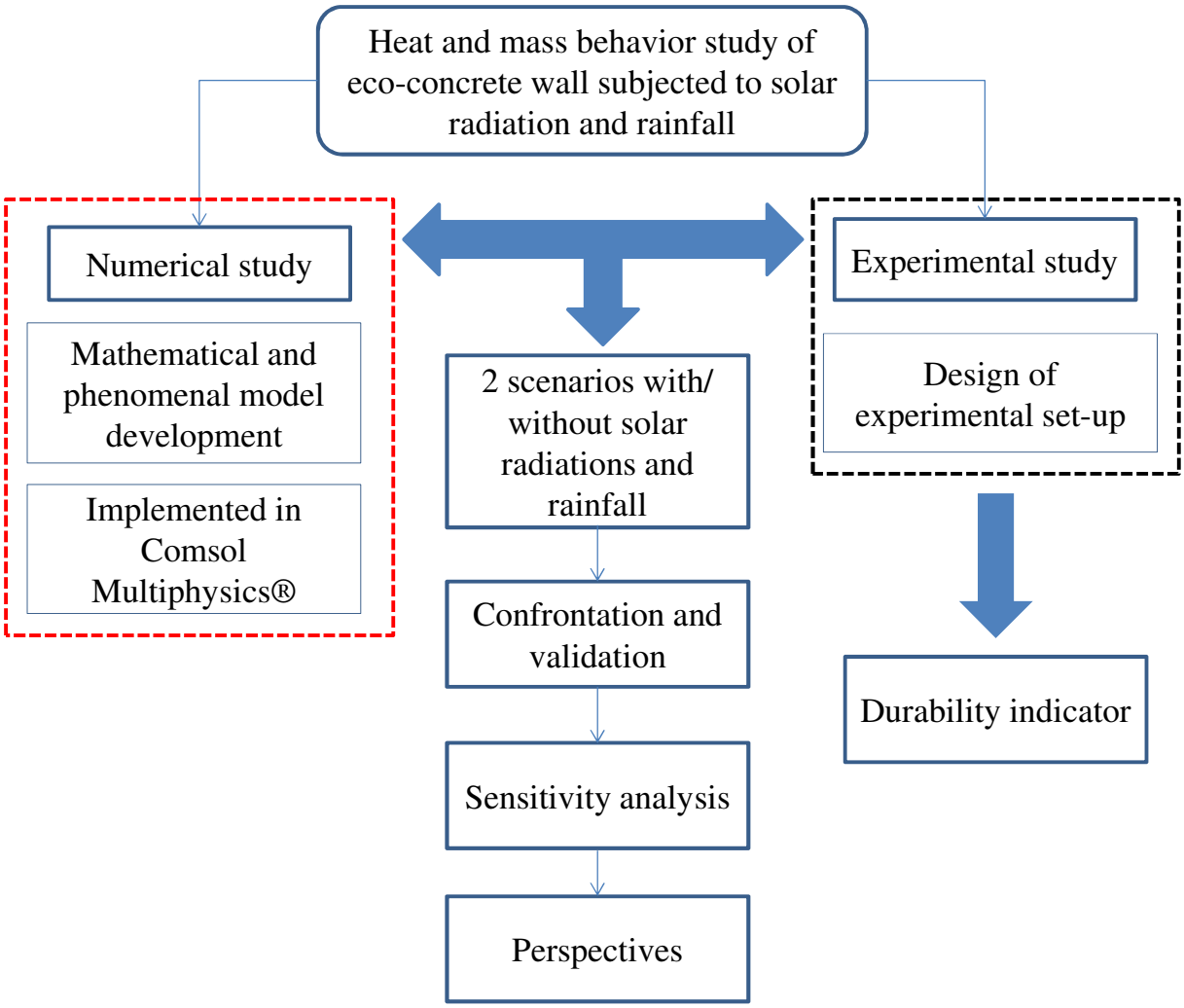

Fig. 2: Outline of the approach undertaken.

2 Experimental set-up

To study the effect of wetting/drying by rainfall/solar radiation on the hygrothermal behavior at the scale of the building wall, a new experimental bench was developed as shown in Fig. 2. It is composed of two cubic chambers with sides of of 1.25 m length and made of 10 mm thick plywood panels with 5 cm of extruded polystyrene insulation on the inside. The water barrier is provided by PVC panels.

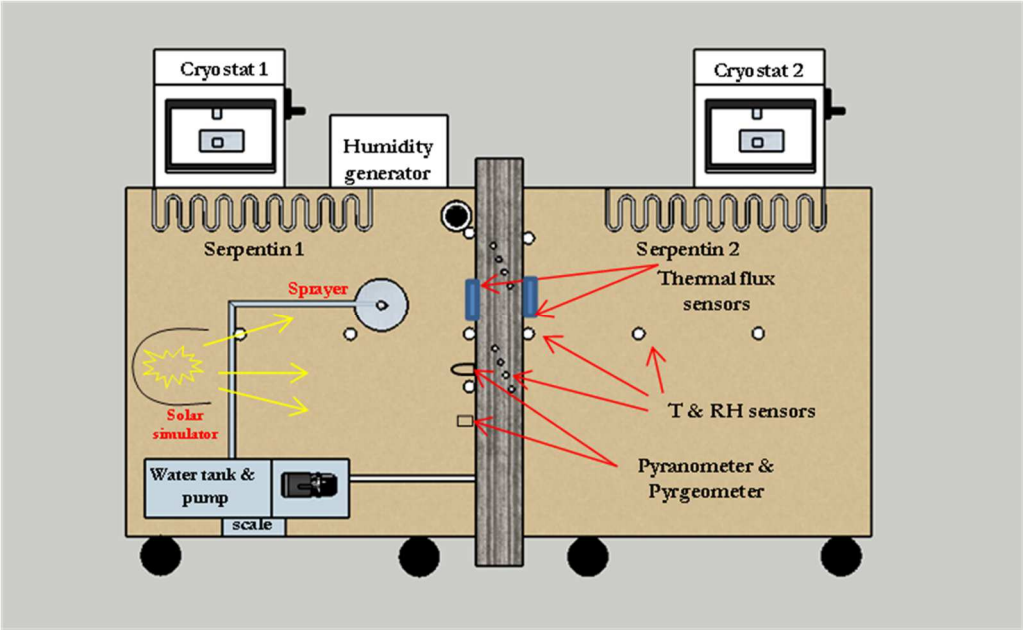

Fig. 2: Experimental bench.

2.1 Wall installation

The studied monolayer wall, with dimensions 1.30 m x 1.35 m x 0.11 m, is shown in Fig. 3. It is made of an eco-concrete with a 20% substitution of cement by glass powder. The wall was built by pouring the eco-concrete in three layers given the large quantity of concrete in an environment of laboratory at 22°C and 60% relative humidity. A concrete vibrator was used to eliminate the effect of segregation and homogenize all the proprieties. The wall was then demolded after 24 hours of curing and conditioned in the same climate as the previous one as shown in Fig. 3. After demolding, we obtained a homogeneous, smooth and less segregated surface due to the fresh vibration.

Once the formwork has been demolded, the sample requires four steps before starting the tests:

- Installation of the vapor barrier made from aluminum adhesive tape and rock wool on the lateral borders of the wall (air and moisture barrier and thermal insulation to minimize edge effects);
- Drilling of the wall at several depths from one side of the wall sample at 4, 6 and 9 cm;
- Inserting the sensors into the wall and then sealing the contours of the cable passages in the wall using silicone and polyethylene well wrapped with adhesive tape;
- Installation of the experimental bench and pre-conditioning of the wall. The air tightness between wall and bench was ensured by clamping.

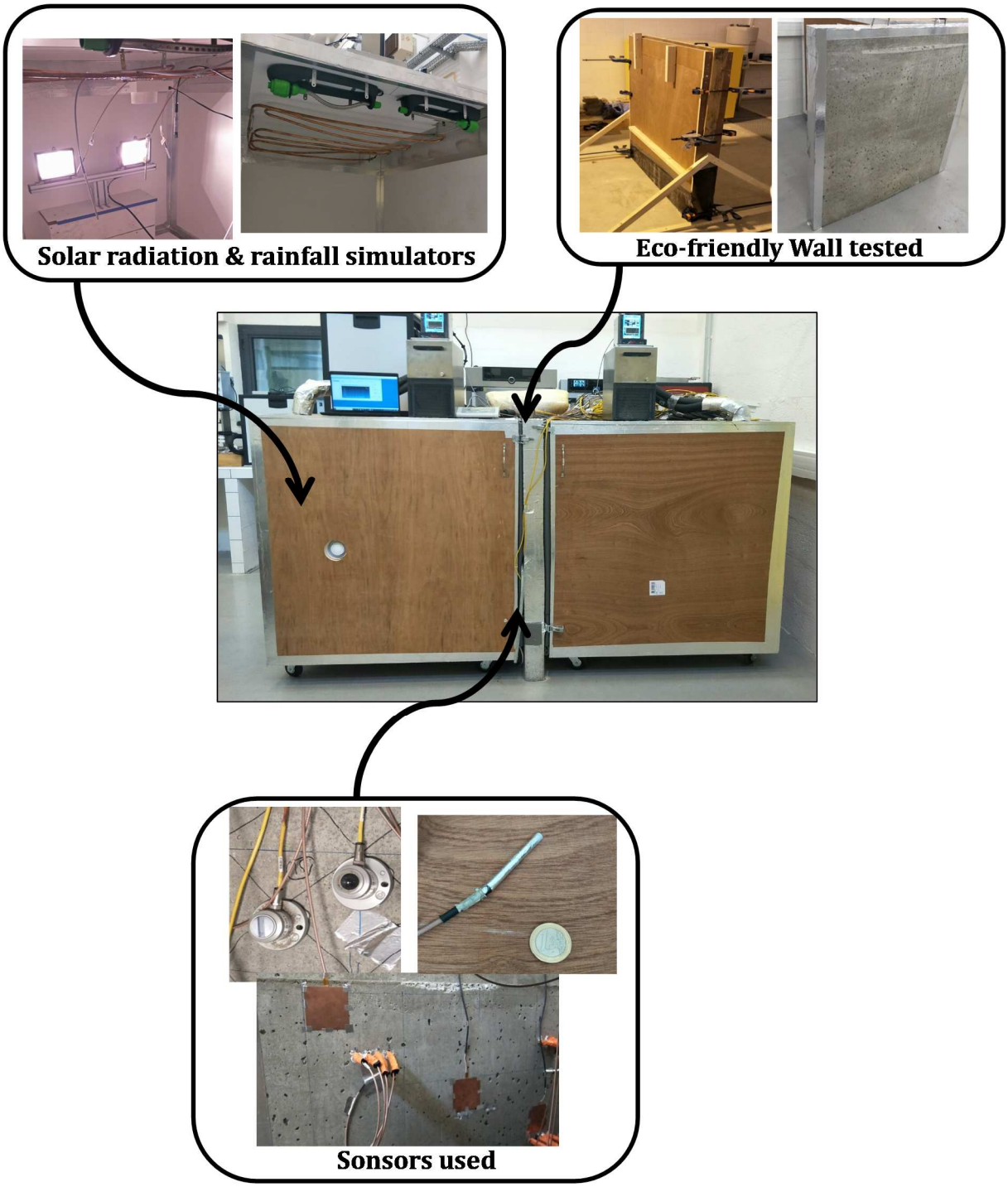

Fig. 3: Bench developed.

2.2 Temperature regulation

Both chambers are temperature-controlled by a temperature bath (Huber temperature baths type CC-K6) with heating and cooling capacities of 2 kW and 0.15 kW respectively. The two temperature baths are connected to a 20m long serpentine pipe, which is installed inside the casing on the upper side to act as a heat exchanger. A fans are installed to circulate the air inside theboth boxes. The boxes are equipped with sensors to regulate and control the temperature. The first box is also equipped with a sprinkler connected to a timer simulating rain and a spotlight simulating solar radiation. The second

chamber simulates the habitable environment. The wall is placed between the two chambers. The wall has humidity and temperature sensors located on the exterior and interior surfaces and through the wall as shown in Fig. 3, and temperature sensors are placed in both chambers at various heights to check the boundary conditions.

2.3 Rainfall simulation

A spraying system is adopted to simulate precipitation. It consists of two sprinklers connected to a pump with a flow rate of 50 l/h which corresponds to a precipitation rate of 50 mm/m²h. The precipitation rate was determined by a simple conversion of the flow rate provided by the pump devided by a surface which is equivalent to 1m² subjected to humidification by the injected water. In fact, this water spray rate is intended to apply uniform and consistent water to the surface of the wall sample, and does not correspond to the amount of wind-driven rain on actual building facades. The pump is immersed in a sealed tank and placed on a Kern® DS 16K0.1 scale with a capacity of 16 kg and a precision of 0.1 g. The latter is connected with a computer for acquisition using Simple Data Logger (SDL) software. The system's power supply is controlled by a timer to regulate the time and rain duration. The purpose of using the scale is to be able to measure the amount of rain absorption by the wall and it corresponds to the rain flow infiltrated by the wind driving rain [32,33].

2.4 Solar radiation simulation

Two Langlois® sun simulators with an electrical power of 500 W each are used to simulate solar radiation. They are installed facing the wall at 60 cm distance, on the same height of 50 cm with an interspace of 45 cm. The facility is connected to an electrical power variator that allows the intensity of light to be varied to simulate solar irradiance ranging from 0 to 1000 W/m² (winter and summer periods). Solar lamps emit in both short and long wavelength radiation (SWL and LWL). Kipp & Zonen® pyranometers and pyrgeometers are installed to measure irradiance in both ranges. These measurements are acquired via an ALMEMO data acquisition system from Ahlborn.

Radiation of the lamp propagate and fall on all the walls of the chamber directedly or by reflection. The homogeneity of the illuminance on the studied wall, in both short and long wavelength has been evaluated (see Fig. 4). The surface map was obtained by installing the pyranometer and pyrgeometer on the surface of the wall at different position following a 5X5 grid. the configuration of the installation generates illuminance heterogeneity, especially for SWL radiation. The central part which is our area of interest shows an acceptable homogeneity.

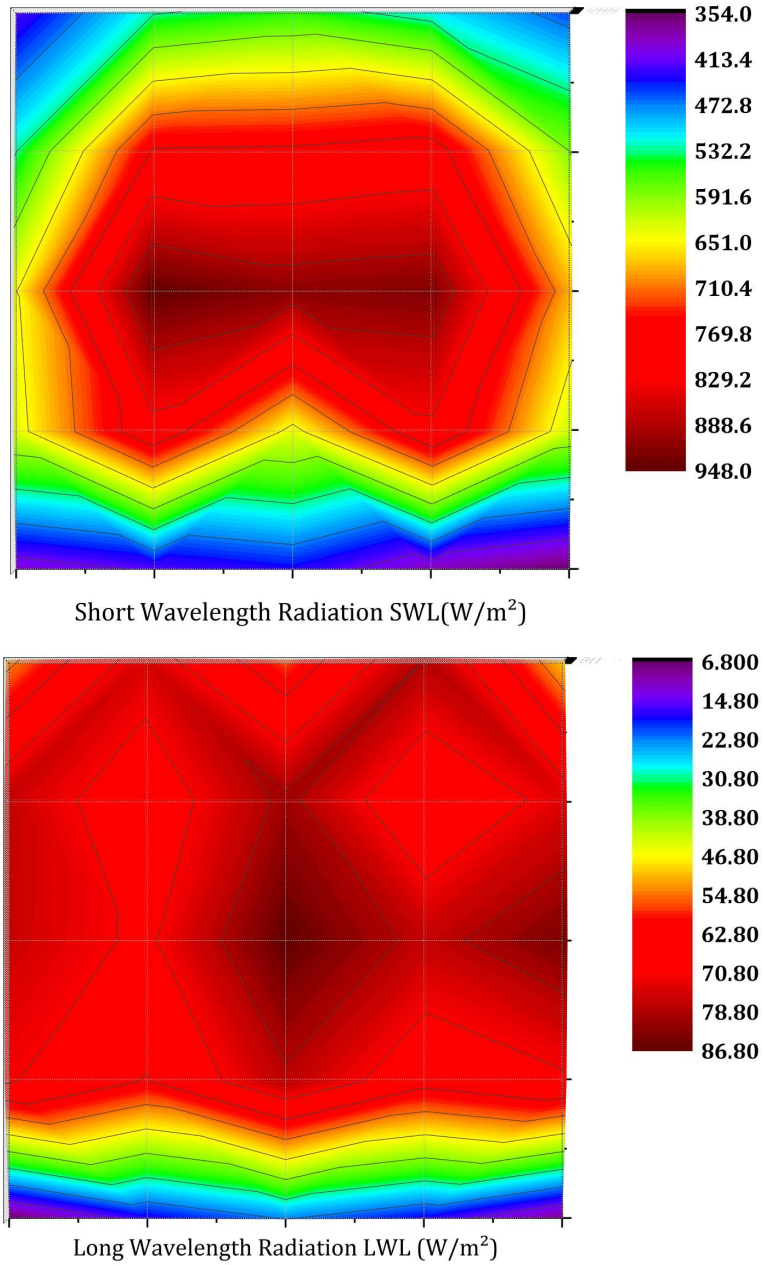

Fig. 4: short and long wavelength radiation distribution on the studied wall

2.5 Further sensors and associated acquisition

The temperature and RH sensors (Ahlborn FHA 646 R) used are thermistor type for T and capacitive type for RH. The advantage of these sensors is their small size and measurement accuracy. They allow the measurement of T and RH in both chambers, at different positions throughout the wall and at the external and internal borders of the wall as shown in Fig. 5. Temperature and relative humidity sensors are placed at 4, 6 and 9 cm and at the external and internal borders. They are installed in depth in 3 different zones. All sensors were pre-calibrated by the manufacturer. They are connected to the ALMEMO data acquisition system. The central station records the data every minute. The characteristics of the sensors are presented in Table 1.

Table 1. The technical data of the hygrothermal and thermal flux sensors

Technical data	
RH accuracy	± 5 %
T accuracy	0.3 °C
Maximum response time	10 s
RH measurement range	0 – 100 % RH
T measurement range	- 20 – 100 °C
Thermal flux sensitivity	60 µV/(W.m^{-2})
Thermal flux range	± 1500 W.m^{-2}
Thermal flux accuracy	5%

The thermal flow meters were calibrated by the manufacturer and are diagonally placed on both borders of the wall to measure the heat flow and connected to a Campbell Scientific datalogger. The frequency of measurement is the same as the temperature and relative humidity acquisition.

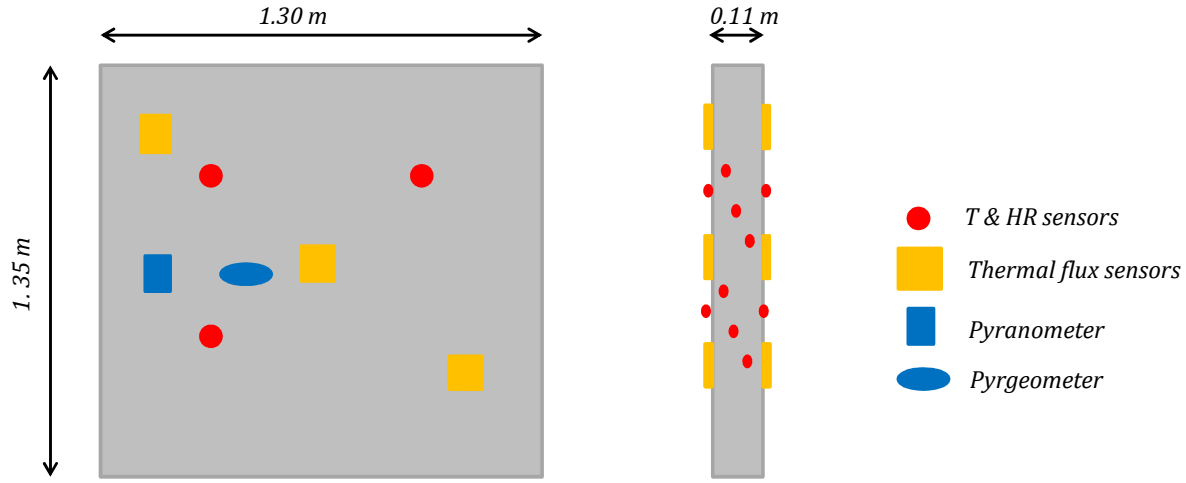

Fig. 5: Sensor position on the wall borders and in the interior of the wall (left external border, right cross-sectional view)

3 Mathematical model of mass and heat transfer in porous media

The development of macroscopic models of coupled heat and moisture transfer to predict the behavior of porous materials has been of interest to several researchers. In this section, a mathematical model based on the Luikov model [12] is proposed for the prediction of the hygrothermal behavior of building walls exposed to rain. The model developed takes the temperature and vapor pressure as transfer potentials. All these input parameters (thermal conductivity λ, specific heat C_p, density ρ, sorption isotherm C_m and water vapor and liquid permeabilities δ_p and k_l) are obtained from existing

research [45]. The water diffusivity D_w is proposed in the literature and is a function of liquid water permeability and water vapor permeability. The measurement campaign carried out is presented in Table 2.

3.1 Mathematical formulation

Moisture transfer in a porous medium can be divided into the diffusion of water vapor and by a capillary effect. Heat transfer is effected by advection conduction [46]. The model developed consists of two heat and moisture balance equations and is based on the following assumptions made in order to simplify some phenomena:

- The solid phase is considered homogeneous, isotropic and non-reactive (the hydration of the cement matrix is assumed to be complete, therefore the source terms due to chemical reactions are neglected);
- The liquid phase is assumed to be pure water;
- The gaseous phase, consisting of dry air and water vapor, follows the perfect gas law;
- Heat transfer by volume radiation is not taken into account, unlike surface radiation;
- Change of the humidity state from liquid or gaseous to solid or vice versa is not considered in this model (freeze/thaw phenomenon);
- Moisture transfer under the gravitational effect is negligible.

3.1.1 Mass balance

Equation 1 represents the mass conservation equation [27]:

$$\frac{\partial w}{\partial t} = -\vec{\nabla}.\left(-\delta_p \vec{\nabla} P_v - k_l \vec{\nabla} P_c\right) \quad (1)$$

where δ_p and k_l are the water vapor permeability and water liquid permeability respectively.

By introducing the isothermal curve into the mass balance equation, the following equations are obtained [47]:

$$C_m \rho_s \left(\frac{1}{P_{v,sat}(T)} \frac{\partial P_v}{\partial t} + P_v \frac{\partial \left(1/P_{v,sat}(T)\right)}{\partial t} \right) = -\vec{\nabla}\cdot\left(-\delta_p \vec{\nabla} P_v - k_l \vec{\nabla} P_c\right) \quad (2)$$

where C_m is the moisture capacity.

Considering the hypothesis of a local thermodynamic equilibrium at the pore level between the two phases (vapor and liquid), Kelvin's law as in Eq. (3) is applicable:

$$P_c = \frac{\rho_l RT}{M} \ln\left(\frac{P_v}{P_{v,sat}(T)}\right) \quad (3)$$

where ρ_l [kg/m^3] is the density of water in liquid state, R [J/(mol·K)] is the perfect gas constant, T [K] is temperature, and M [kg/mol] is the molar mass.

In addition, it is known that the relative humidity (RH) can be described with the following equation:

$$RH = \frac{P_v}{P_{v,sat}(T)} \quad (4)$$

To determine the capillary pressure gradient, Eq. (3) must be derived to transform the capillary pressure gradient into a combination of a water vapor pressure gradient and a temperature gradient, which gives:

$$\vec{\nabla} P_c = \frac{\rho_l R}{M} \ln\left(\frac{P_v}{P_{v,sat}(T)}\right)\vec{\nabla} T + \frac{\rho_l RT}{M} \frac{\partial \ln\left(\frac{P_v}{P_{v,sat}(T)}\right)}{\partial T}\vec{\nabla} T + \frac{\rho_l RT}{MP_v}\vec{\nabla} P_v \quad (5)$$

The mass transfer equation is written as follows:

$$\frac{C_m \rho_s}{P_{v,sat}(T)} \frac{\partial P_v}{\partial t} = \vec{\nabla}\cdot\left(K_{PP}\vec{\nabla} P_v + K_{PT}\vec{\nabla} T\right) + \frac{C_m \rho_s P_v}{P_{v,sat}(T)^2} \frac{\partial P_{v,sat}(T)}{\partial T} \frac{\partial T}{\partial t} \quad (6)$$

where

$$K_{PP} = \left(\delta_p + k_l \frac{\rho_l RT}{MP_v}\right) \quad (7)$$

$$K_{PT} = k_l \left(\frac{\rho_l R}{M} \ln\left(\frac{P_v}{P_{v,sat}(T)}\right) + \frac{\rho_l RT}{M} \frac{\partial \ln\left(\frac{P_v}{P_{v,sat}(T)}\right)}{\partial T} \right) \quad (8)$$

3.1.2 Energy balance

Heat transfer in porous wet materials is governed by the energy conservation equation (Eq. 9) involving conduction heat transfer in the solid and liquid phases governed by Fourier's law [34], convective heat transfer in the liquid and gaseous phases, and liquid-gas phase change [48].

$$C_p \rho_s \frac{\partial T}{\partial t} = -\vec{\nabla}\cdot\left(\vec{j_q}\right) \quad (9)$$

where C_p is the heat capacity and ρ_s is the dry density.

Heat flow is written as follows [49]:

$$\vec{j_q} = -\lambda\vec{\nabla} T + h_l \vec{j_l} + h_v \vec{j_v} \quad (10)$$

where λ is the thermal conductivity, h_l is the mass enthalpy of liquid water (J/kg), h_v the mass enthalpy of water vapor (J/kg), j_l is the liquid flow density (kg/m^2.s) and j_v is the vapor flow density (kg/m^2.s).

The heat transfer equation will be:

$$C_p\rho_s\frac{\partial T}{\partial t}=-\vec{\nabla}\cdot\left(-\lambda\vec{\nabla}T-h_l\left(k_l\vec{\nabla}P_c+\delta_p\vec{\nabla}P_v\right)\right)+L_v\sigma C_m\frac{\rho_s}{P_{vsat}(T)}\frac{\partial P_v}{\partial t} \quad (11)$$

where L_v is the latent heat of vaporization (J/kg) and σ=div (j_v) / div (j_l+j_v).

Grouping the values in terms of temperature and vapor pressure will give:

$$C_p\rho_s\frac{\partial T}{\partial t}=\vec{\nabla}\cdot\left(K_{TT}\vec{\nabla}T+K_{TP}\vec{\nabla}P_v\right)+L_v\sigma C_m\frac{\rho_s}{P_{vsat}(T)}\frac{\partial P_v}{\partial t} \quad (12)$$

where

$$K_{TT}=\left(\lambda+h_lk_l\frac{\rho_lR}{M}\ln\left(\frac{P_v}{P_{v,sat}}\right)+h_lk_l\frac{\rho_lRT}{M}\frac{\partial\ln\left(\frac{P_v}{P_{v,sat}}\right)}{\partial T}\right) \quad (13)$$

$$K_{TP}=\left(h_l\delta_p+k_lh_l\frac{\rho_lRT}{MP_v}\right) \quad (14)$$

Both the heat and mass transfer equations can be written in condensed form, as follows:

$$\rho_s\begin{bmatrix}C_m & 0\\ 0 & C_p\end{bmatrix}\begin{Bmatrix}\frac{\partial P_v}{\partial t}\\ \frac{\partial T}{\partial t}\end{Bmatrix}=\vec{\nabla}\cdot\begin{bmatrix}K_{PP} & K_{PT}\\ K_{TP} & K_{TT}\end{bmatrix}\begin{Bmatrix}\vec{\nabla}P_v\\ \nabla T\end{Bmatrix}+\begin{Bmatrix}\frac{C_m\rho_sP_v}{P_{v,sat}(T)^2}\frac{\partial P_{v,sat}(T)}{\partial T}\frac{\partial T}{\partial t}\\ L_v\sigma C_m\frac{\rho_s}{P_{vsat}(T)}\frac{\partial P_v}{\partial t}\end{Bmatrix} \quad (15)$$

3.2 Numerical solution

Numerical simulation of highly coupled mass and heat transfers is carried out by the prediction model represented by the system of partial differential equations PDEs (Eq. 15). The numerical implementation of the model requires a powerful solver environment allowing the treatment of multi-physical problems where several phenomena are studied simultaneously. Therefore, COMSOL multiphysics® provides interfaces and a selection of mathematical algorithms for modeling and solving multiphysics problems via calculation code based on the finite element FE method [50]. It is widely used in the scientific community, particularly for the type of multi-physics problem that concerns us.

The physics used to solve the coupled system of equations is the mathematical module under the general form PDEs. First, the material properties depending on the state variable are defined as

interpolation functions and the different constants and coefficients of the model are also defined. Both in terms of complexity and computational cost, it would be beneficial to have a simplified 1D model. This is considered justified, for two reasons: (1) Mass and heat transfer using the experimental setup is stipulated to be unidirectional due to the use of water and thermal insulation in the wall edges; (2) research has shown that, despite the spatial variability of wind-driven rain distribution across walls and in the absence of runoff, the redistribution of humidity in the plane of the wall is limited, and 1D heat and mass modelling is sufficiently accurate (except for very heterogeneous walls such as masonry) [51]. Then, the boundary and initial conditions were also defined by the interpolation functions. They are those measured experimentally by the sensors installed in the external/internal borders and through the wall.

Beyond that, the PDEs domain are meshed in space using the FE method. This latter is performed and controlled automatically by the solver with a very fine size of order of 0.0011 m. For time setting, the implicit Backward Differentiation Formulas (BDF) method has been chosen with adaptative mesh and maximal time step of 1 minute. The Multifrontal Massively Parallel Sparse MUMPS direct solver has been selected to solve the linear system. In addition, the fully coupled system given by Eq.15 has been solved simultaneously by the fully coupled mode. In fact, each time step yields a non-linear equation system that is linearized and iteratively solved by Newton's method [52]. The convergence criteria chosen is of order 1e-4 for each time step. The time-dependent solver calculates the solution of a possibly non-linear system of equations at each time step via a set of iterative techniques based on Newton's method. These Newton's method used for solving a nonlinear system of equations evaluate a function, as well as its derivative, at each time step. This derivative is also known as the Jacobian and is relatively expensive to calculate. Therefore, the software will try to minimize the re-evaluation of the Jacobian, by preference. If the nonlinear solver has difficulty converging, it will reduce the size of the requested time step and try to calculate the solution as detailed by Beneš et al. [53]. After running the simulation for the specified period, temperature, relative humidity, vapor pressure and heat and mass flows evolutions at any location with all-time steps can be determined.

3.3 Model input parameters

The prediction quality of the heat and mass transfer model requires reliable input parameters. a detailed characterization campaign of the hygrothermal transfer parameters is established and grouped in Table 2. In fact, the use of glass powder as a partial replacement of portland cement CEMI, of about 20 %, allows to change the microstructure by creating micropores of order lower than 0.01 µm as well as macropore of order higher than 100 µm. This change of the pore size induces an increase of the total porosity of the material about 14.18 % compared to a reference concrete with a porosity of 13.14 %. This means a decrease in thermal conductivity by 3.7 % and specific heat by 1.4 %. Regarding the mass transfer parameters, the incorporation of GP in concretes increases their moisture storage capacity by 20% and its dry vapor permeability 2 times more compared to the control concrete [54].

As for the wet water vapor permeability and the liquid water permeability, these are estimated by using the inverse method based on gradient descent and reported in [45].

Table 2: Properties of studied material [54].

Property	Value & Expression	Identification method & experimental device
Dry thermal conductivity λ_{dry}	1290 [mW.m^{-1}.K^{-1}]	Guarded hot plate method by λ-Meter EP 500e® device [55,56]
Water thermal conductivity λ_{water}	607 [mW.m^{-1}.K^{-1}]	-
Dry specific heat $C_{p\ dry}$	850 [J.kg^{-1}.K^{-1}]	3D Calorimeter Calvet® [57]
Water specific heat $C_{p\ water}$	4400 [J.kg^{-1}.K^{-1}]	-
Density ρ_s	2290 [kg.m^{-3}]	-
Water vapor permeability δ_p	3.38e-11 exp(-5.998RH) [kg.m^{-1}.s^{-1}.Pa^{-1}]	Inverse method [45]
Water liquid permeability k_l	3.493e-13 exp(6.003RH)/RH [kg.m^{-1}.s^{-1}.Pa^{-1}]	Inverse method [45]

The thermal properties in the hydric state are given as below [58]:

$$C_{p\ humid} = C_{p\ dry} + C_{p\ \ water} \cdot u \quad (16)$$

$$\lambda_{humid} = \lambda_{dry} + \lambda_{\ water} \cdot \frac{\rho_s}{\rho_w} \cdot u \quad (17)$$

where u is the water mass content (kg/kg). It is determined by a gravimetric method using a ProUmid SPS® device according to [59]. The sorption isotherm of the tested material is presented by the GAB model [60] and given by Eq. (18), where *m=0.5912; C=9.953* and *K=0.913*.

$$u = \frac{m \cdot C \cdot K \cdot RH}{\left(1 - K \cdot RH\right)\left(1 + K \cdot \left(C - 1\right) \cdot RH\right)} \quad (18)$$

4 Wall scale scenarios and numerical simulation

Two scenarios were performed in this study. In the first one, called "test under sinusoidal effects without solar radiation nor rainfall", we considered sinusoidal conditions in the temperature with alternating episodes of precipitation and radiation. The objective of this test is precisely to study the effect of drying/wetting cycles without solar radiation/rainfall on the one hand, and to investigate the capacity of the model to obtain the same results as the experimental one.

In the second test carried out, called "sinusoidal effects test with solar radiation and rainfall", sinusoidal conditions in the temperature were considered with alternating episodes of rainfall and radiation by varying the air temperature of the outdoor chamber according to a sinusoidal type signal. The objective of this test is to investigate the capacity of the model to predict the hygrothermal behavior of the wall.

Accordingly, Dirichlet boundary conditions are considered for the numerical calculation. The measurements provided by the sensors at x=0 and 11 cm are used to describe the temperature and relative humidity at the exterior and interior edges.

The mean error (ME) and the root mean square error (RMSE) were used to assess the consistency of the numerical results with the experimental datas.

$$\mathrm{ME} = \frac{\sum_{i=1}^{n} \left| y_{meas} - y_{num} \right|}{n} \quad (19)$$

$$\mathrm{RMSE} = \sqrt{\frac{\sum_{i=1}^{n} \left(y_{meas} - y_{num} \right)^2}{n}} \quad (20)$$

where y_{meas} is the experimental measured values, y_{num} is the numerical model results and n is number of values.

4.1 Test without solar radiation nor rainfall (Test 1)

Three hygrothermal sensors are installed in the two chambers. The temperature T and Relative Humidity RH variations of the room during the Test 1 are shown in Fig. 6. The T/RH and vapor pressure Pv evolution in the two chambers is shown in Fig. 7 and Fig. 8, respectively. We note that the two chambers are well insulated in relation to the room's climate. In the outdoor chamber, the temperature condition is sinusoidal, varying from 25 to 15 °C with a period of 1 day and this for a total period of 7 days. While it is constant in the internal compartment with a temperature equal to 20 °C. The humidity was left to evolve freely in the two chambers without the use of a humidity generator. An increase in the Pv in both chambers is observed. This is due to the interaction between the wall and the both chamber atmosphere. The RH values decrease as temperature increase in single cycles, while the overall trends in RH increase with time due to release of water vapor from the wall.

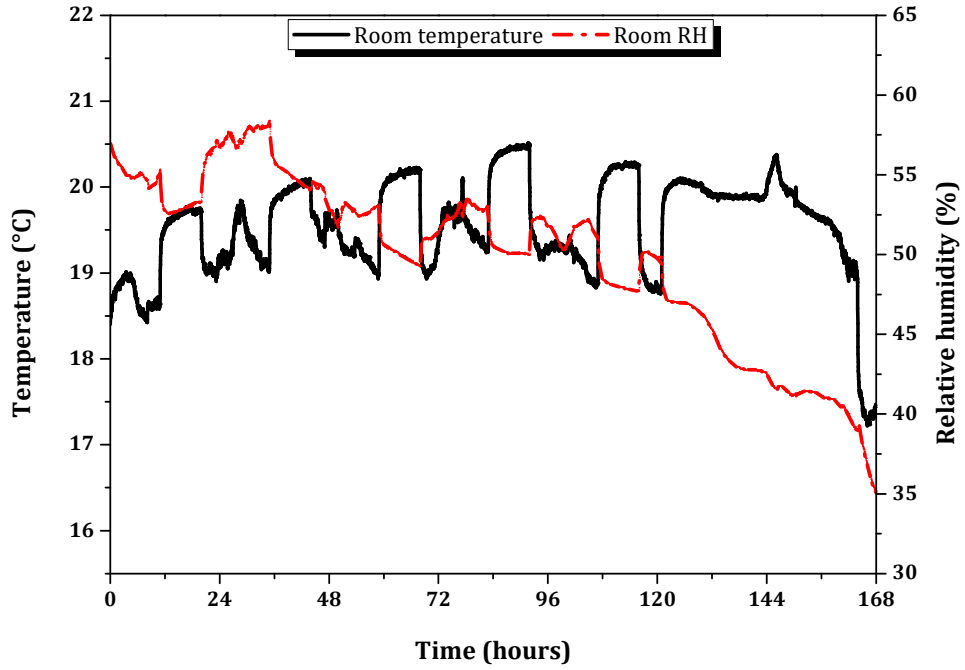

434

435 Fig. 6: T and RH of the room during the Test 1.

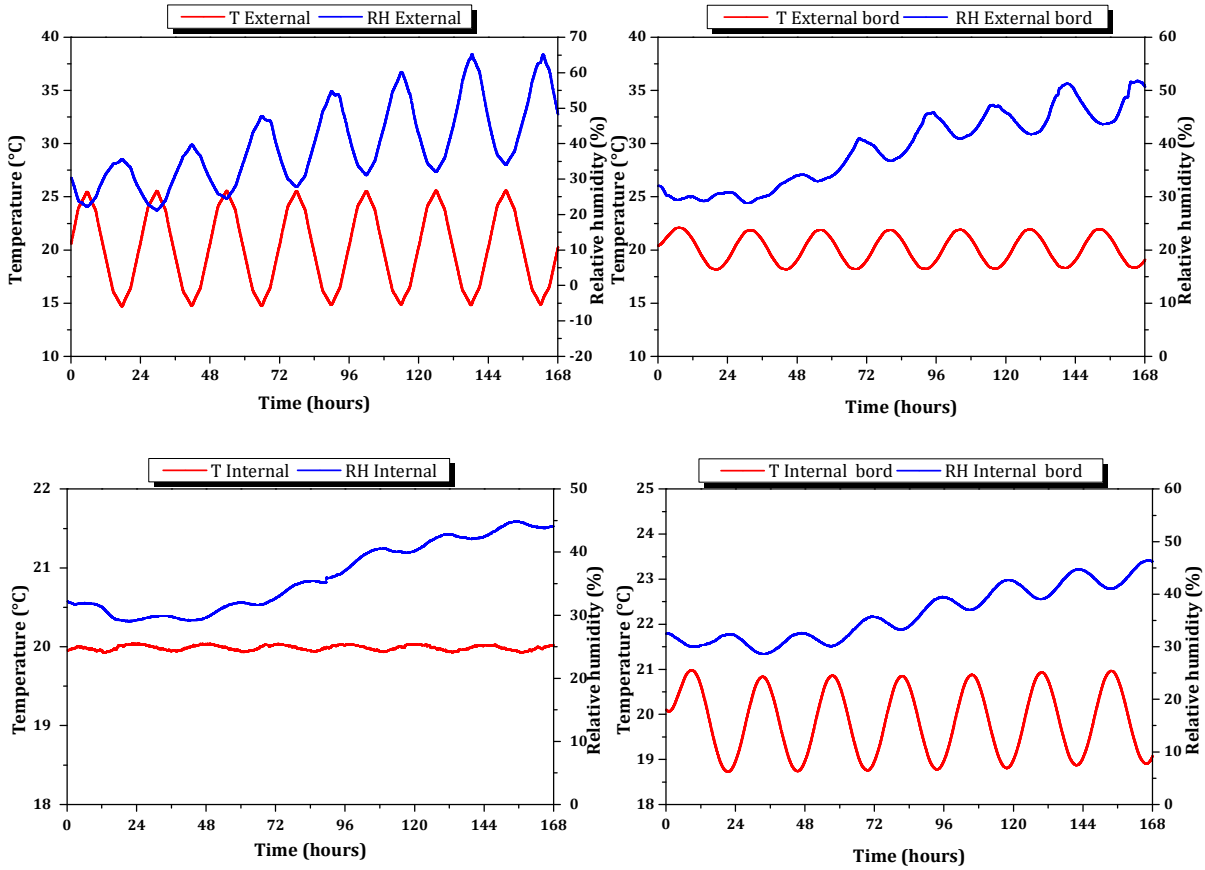

436

437

438 Fig. 7: Temperature conditions and relative humidity variation in the outdoor/indoor chambers &
439 external/internal borders.

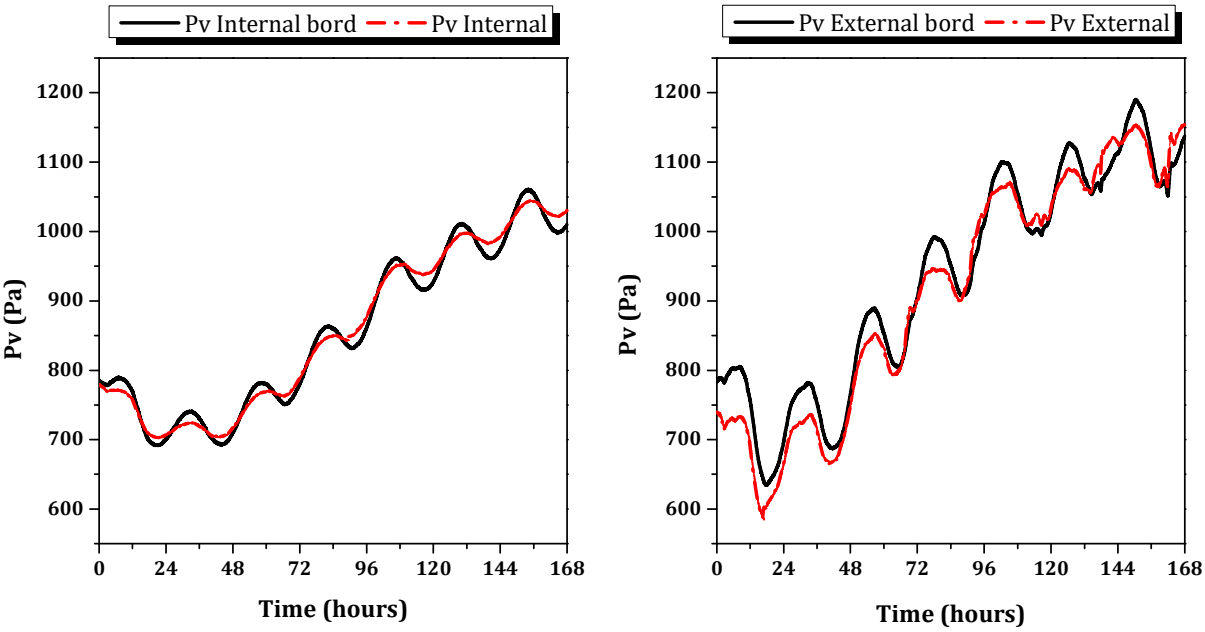

440

441 Fig. 8: Vapor pression in the outdoor/indoor chambers & external/internal borders.

442

443 The temperature evolution within the wall at different depths is shown in Fig. 9Fig. . The temperature
444 variation in the outdoor chamber generates a variation in temperature and an increase in the relative
445 humidity in the wall. In fact, the absolute temperature difference does not exceed 0.3 °C and it remains
446 within the margin of error of the sensor used (see Table 1). The largest errors are recorded at the time
447 of signal changing the outdoor chamber temperature. A good correlation between the experimental and
448 numerical values are recorded with R^2= 0.9547, 0.9788 and 0.9668 at 4, 6 and 9 cm, respectively.

449 In addition, the stability of the relative difference is noted between the experimental and numerical
450 measurements, with an absolute deviation of the magniture of 2%, 1% at 4 and 6cm and 5% at 9cm as
451 shown in Fig. 10. Generally, a good prediction of RH through the wall is obtained using the proposed
452 numerical model compared with the results from the experimental simulation. Table 3 shows the MEs
453 and RMSEs between the numerical and experimental relative humidity/temperature at the depth of 4, 6
454 and 9 cm. Numerical and experimental results have the maximum MEs which are 0.22 °C and 3.02 %,
455 for the temperature and relative humidity, respectively. Furthermore, Numerical and experimental
456 results have the maximum RMSEs of temperature and relative humidity which are 0.24 °C and
457 4.78%, respectively.

458 This analysis has shown certain deviations between the experiment and numerical simulation,
459 especially in the case of dynamic loads and during the time of relative humidity signal variation.
460 However, these were not demonstrated clearly by literature and required further investigation [61].
461 The deviations found may be related to several factors, in the one hand, the numerical solution of the
462 prediction model (the choice of the solver, adequate mesh and the solution scheme), the formulation of
463 the phenomenological models of hygrothermal transfers (the non-inclusion of certain physical
464 phenomena) and the measurement uncertainties resulting from the experiment (sensor error and the
465 impact of the environment on the measurement), and in the other hand, it may be related to the
466 variability of the properties of the material used [62].

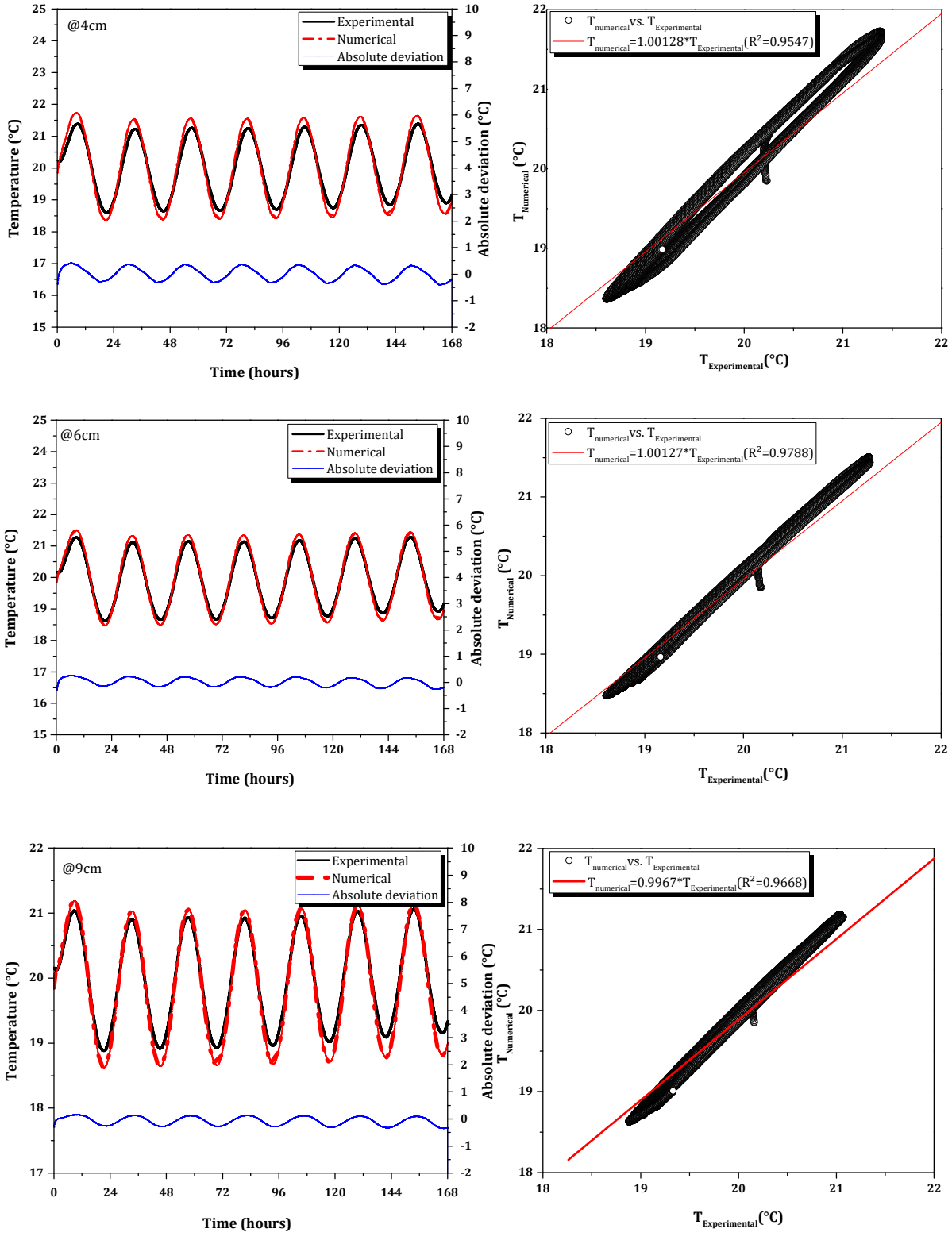

Fig. 9: Temperature evolution at 4, 6 and 9 cm.

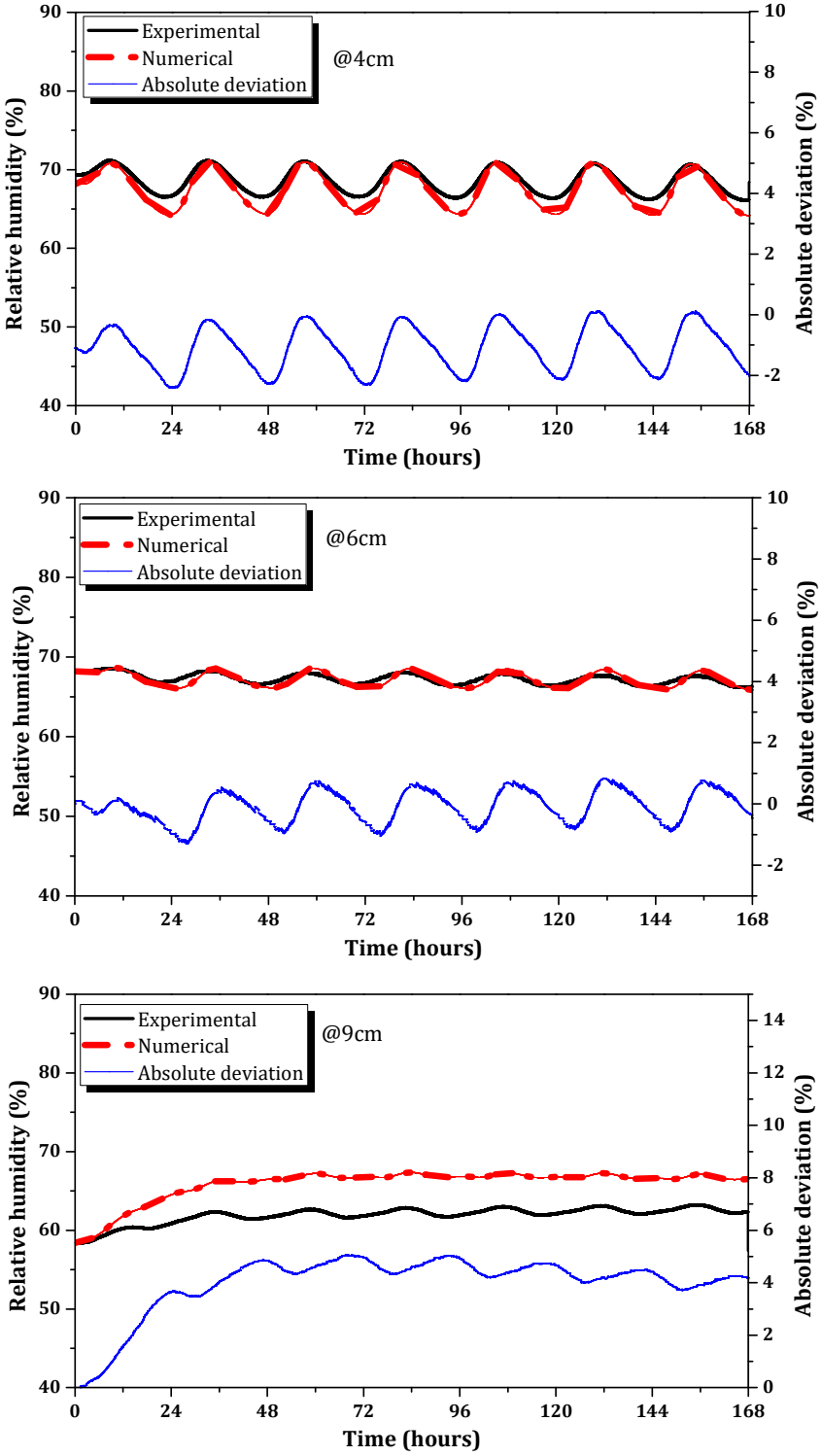

Fig. 10: Relative humidity evolution at 4, 6 and 9 cm.

In addition, the heat flux measurements were performed on the external and internal borders as shown in Fig. 11. The simulated heat flux is in good agreement with the measured flux. Indeed, a very good correlation between our experimental observation and the results of the numerical simulation can be seen with R^2=0.8864 and 0.9408 for the external/internal border, respectivly. However, the simulated flux at the external and internal borders is underestimated by 2.3% and overestimated by 10%

respectively, compared with the values measured experimentally. The MEs and RMSEs between the numerical and experimental thermal flux at the external/internal borders are shown in Table 3. The results have the maximum MEs which is 1.7 and 0.98 $W.m^{-2}$, at external/internal borders, respectively. Furthermore, the RMSEs of being about 2.28 and 1.41 $W.m^{-2}$ at the external/internal borders, respectively. The numerical results of the model are in a good agreement with the measured data.

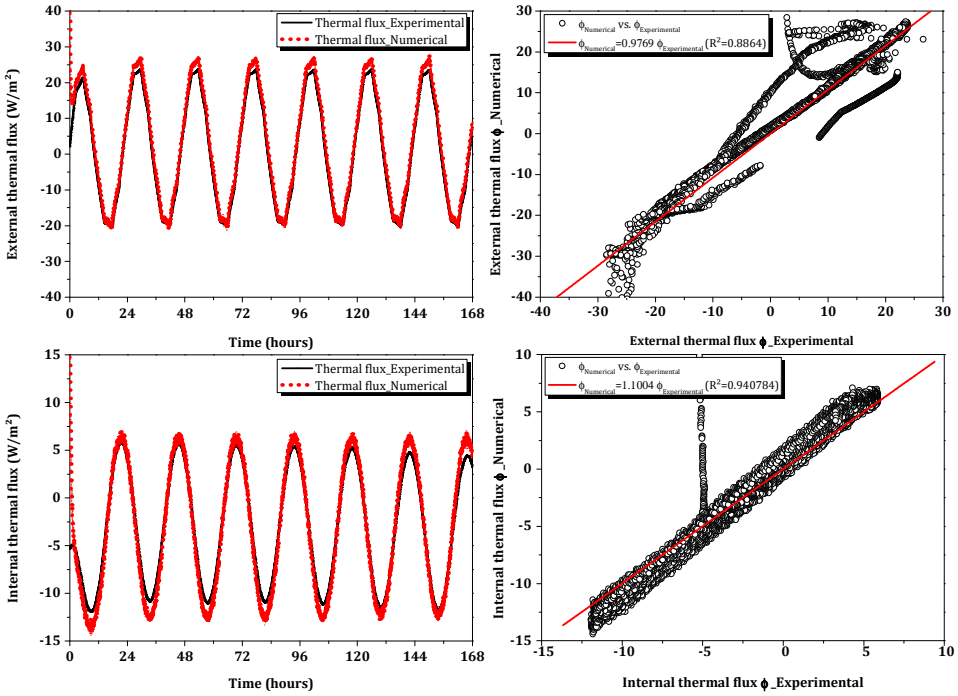

Fig. 11: Comparison of the conducted heat flux of the model prediction with the experimentally measured heat flux at the external and internal borders.

Table 03: MEs and RMSEs between experimental and numerical results

		x=0	x=4cm	x=6cm	x=9cm	x=11cm
T [°C]	ME	-	0.22	0.13	0.14	-
	RMSE	-	0.24	0.15	0.17	-
RH [%]	ME	-	1.50	1.82	3.02	-
	RMSE	-	2.96	3.47	4.78	-
J_q [$W.m^{-2}$]	ME	1.70	-	-	-	0.98
	RMSE	2.28	-	-	-	1.41

4.2 Test with solar radiation and rainfall (Test 2)

The T and RH variations of the room during the Test 2 are shown in Fig. 12. The sinusoidal loadings are used to get closer to the real conditions to which a building's walls are subjected. While respecting the operating range of the climatic chamber, a configuration has been chosen that shows the variations in T/RH, Pv and SWL/LWL solar radiation and rainfall as shown in Figs. 13, 14 and 15, respectively. The two chambers built are well insulated from the climate of the room, both in temperature and humidity. The temperature fluctuates between 28 and 15°C and a temperature peak is observed during the radiation period due to the Joule effect. In fact, when applying solar radiation, the lamps heat the

internal air circulating in the chamber which is in contact with the hot surfaces of the lamps by convective exchange [63]. The observed decrease in RH and an increase in Pv values was related to the increase in temperature in the drying chamber over the duration of the experiment [64], after that, an increase in RH is observed during the rainfall application due to the humidification of air by the water rain. In addition, the variation of RH and Pv in the indoor chamber is partly due to the interaction between the wall and the chamber atmosphere.

With regard to the evolution of the relative humidity, maximum values are observed during the precipitation periods and minimum values during the radiation periods. The average flow of rain infiltrated during the rainfall sequence was measured and is of the magnitude of 288 g/m².h. With regard to solar radiation, the average radiative fluxes are of the magnitude of 820 W/m² for short wavelength illuminances and about 75 W/m² for long wavelength illuminances, as shown in Fig. 14. These values were obtained for the whole sequence of solar irradiation.

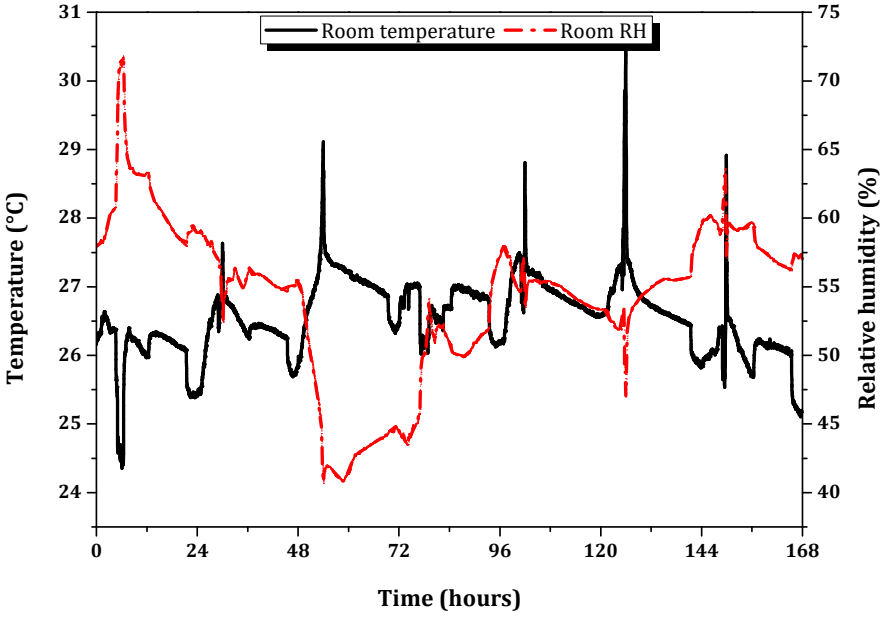

Fig. 12: T and RH of the room during the Test 2.

In the second compartment simulating the building environment, the temperature was set at 20 °C. And following the evolution of the relative humidity inside as shown in Fig. 13, a slight fluctuation is observed in the temperature measurement due to the temperature variation in the outdoor chamber. In addition, a slight increase in the relative humidity in the indoor chamber is also observed due to the interaction of the wetted wall with the indoor chamber during the precipitation phase.

516

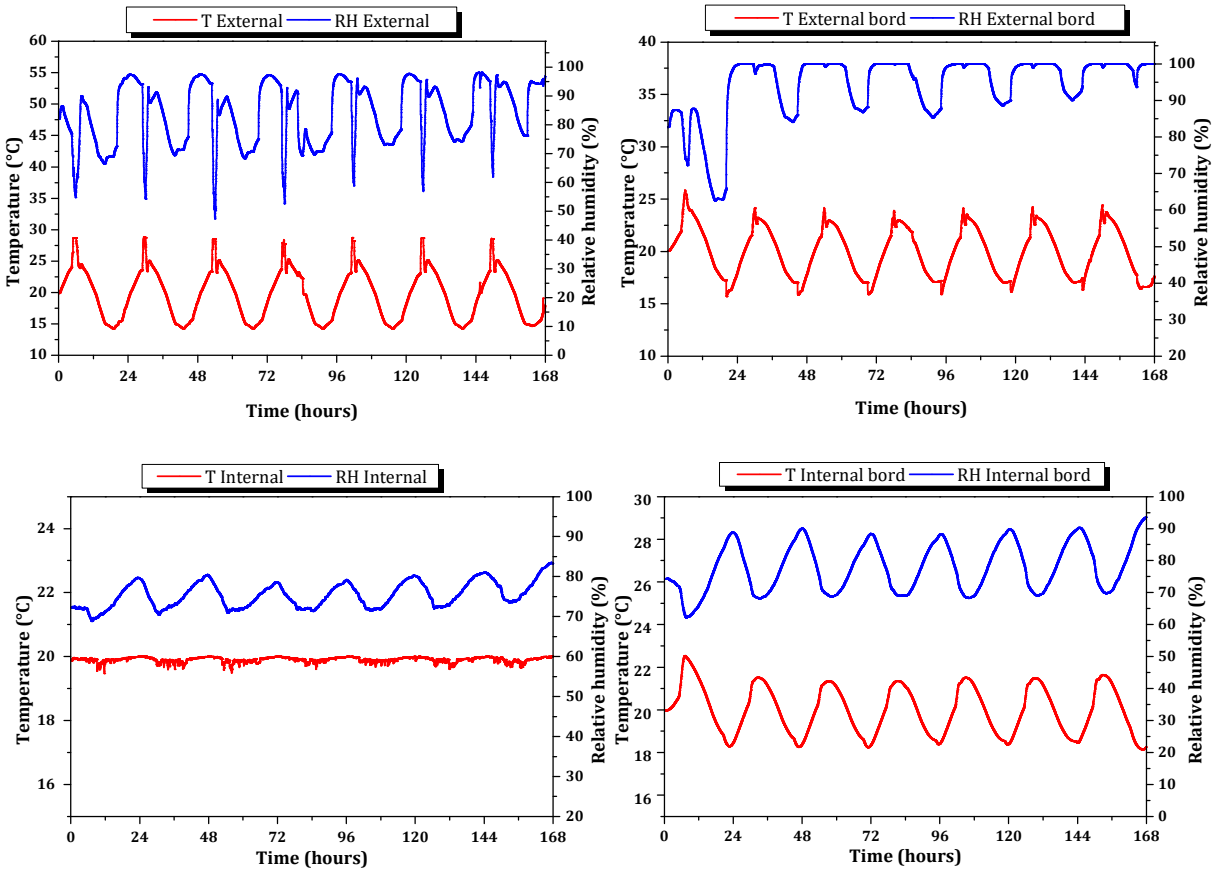

517

518 Fig. 13: Temperature conditions and relative humidity variation in the outdoor/indoor chambers &
519 external/internal borders.

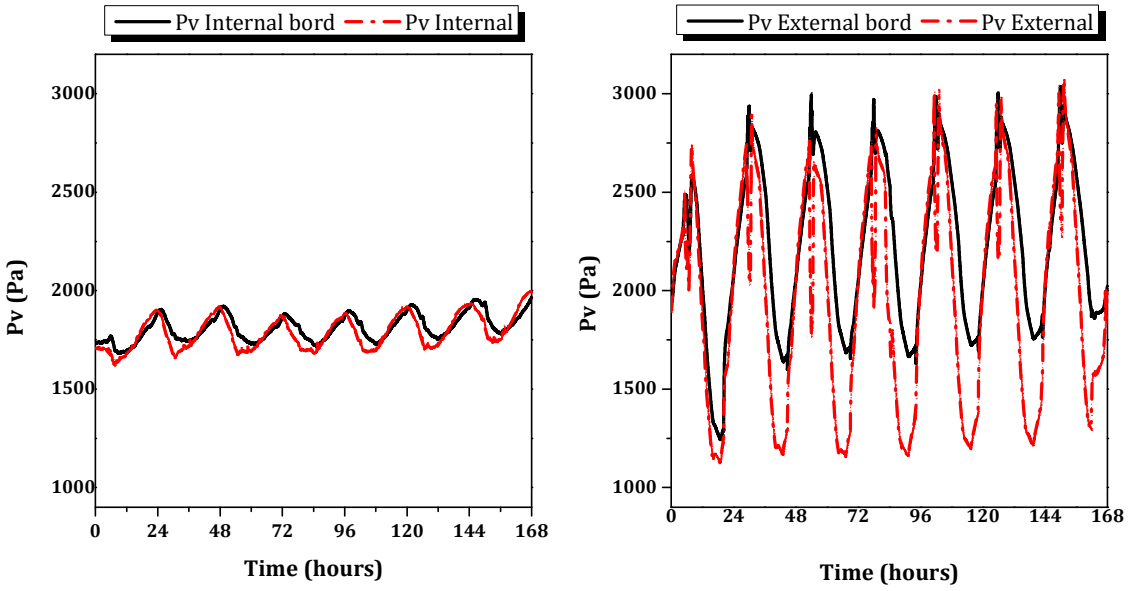

Fig. 14: Vapor pression in the outdoor/indoor chambers & external/internal borders.

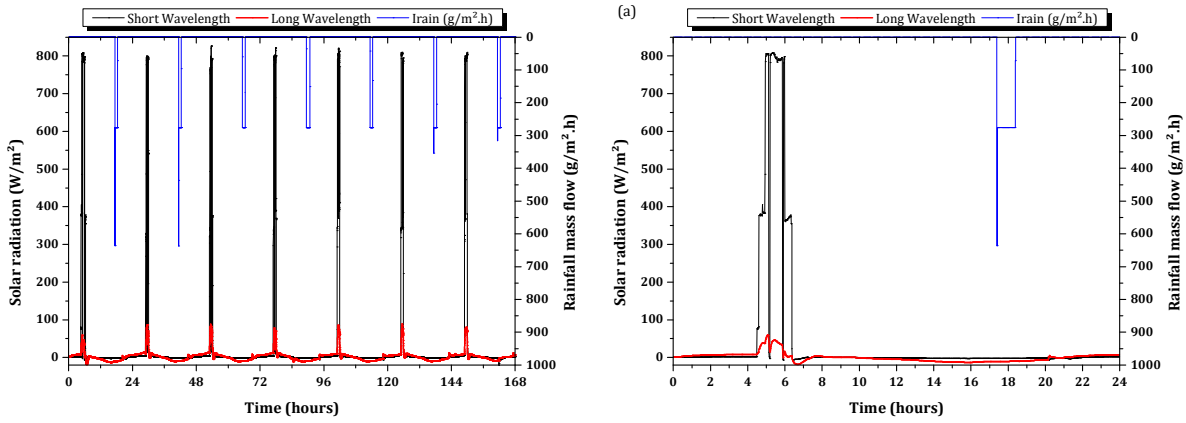

Fig. 15: The flow of radiation and rainfall infiltrated in the wall (external border): (a) representation of the sinusoidal sequence; (b) a zoom on a single period.

The hygrothermal behavior of the wall exposed to sinusoidal loading is presented at several depths: 4, 6 and 9 cm. On the thermal transfer part, the temperature evolution in the wall can be seen in Fig. 16. The temperature varies in time between 26 and 14 °C. Indeed, the thermal wave imposed on the external side propagates in the wall and induces a response in phase with an amplitude that becomes more and more attenuated as one moves away from the external border. This begins with a period of drying by solar radiation. Therefore, the amplitude of the first sequence is greater than the remaining ones by about 1.5 °C, 1.3 °C and 0.9 °C at 4, 6 and 9 cm respectively. After that, the wall studied is subjected to cooling during the rainfall periods, and subsequently the amplitude of the response of the wall to the imposed conditions is reduced. In addition, the largest errors are recorded at the time of the temperature signal change in the outdoor chamber and the application of solar radiation and rainfall periods, but these always remain within the error range of the sensors used. A good correlation

between the experimental and numerical values are recorded with R^2 = 0.978, 0.9827 and 0.9838 at 4, 6 and 9 cm, respectively.

On the mass transfer part, the oscillations of the RH of the wall in time in response to the dynamic conditions is shown in Fig. 17. The largest errors are recorded at the time of the change of temperature and relative humidity in the oudoor chamber. Indeed, during rainfall periods, the wall undergoes a wetting by liquid water. Then, during the application of solar radiation, the wall is dried out. In addition, the stability of the relative difference is noted between the experimental and numerical measurements, with a maximum absolute deviation of the magniture of 4% at 4 and 6 cm, remaining within the tolerance of the sensors used. Indeed, the deviation at 9 cm begins at about 3% and ends at 8% at the end of Test 2. However, the deviation is maximal at the time of the temperature signal change. This is explained by the fact that the relative humidity is dependent on the temperature, and by the effect of hysteresis between the curves of the sorption and desorption isotherms [65]. These results can be related with the water content using the sorption isotherm, that it is the transport vector for aggressive agents such as sulfates, carbonations and chlorides, and which presents an indicator of the sustainability of porous building materials [66].

Table 4 shows the MEs and RMSEs of the numerical and experimental measurement of T/RH. The MEs and RMSEs of T and RH simulated by the present model are very close at each measurement location in the wall. The ME of T/RH at 4, 6 and 9 cm is within the range of 0.14 – 0.20 °C and 1.44 – 3.02 %, whereas the RMSE is within the range of 0.18–0.23 °C and 1.81–3.47 %.

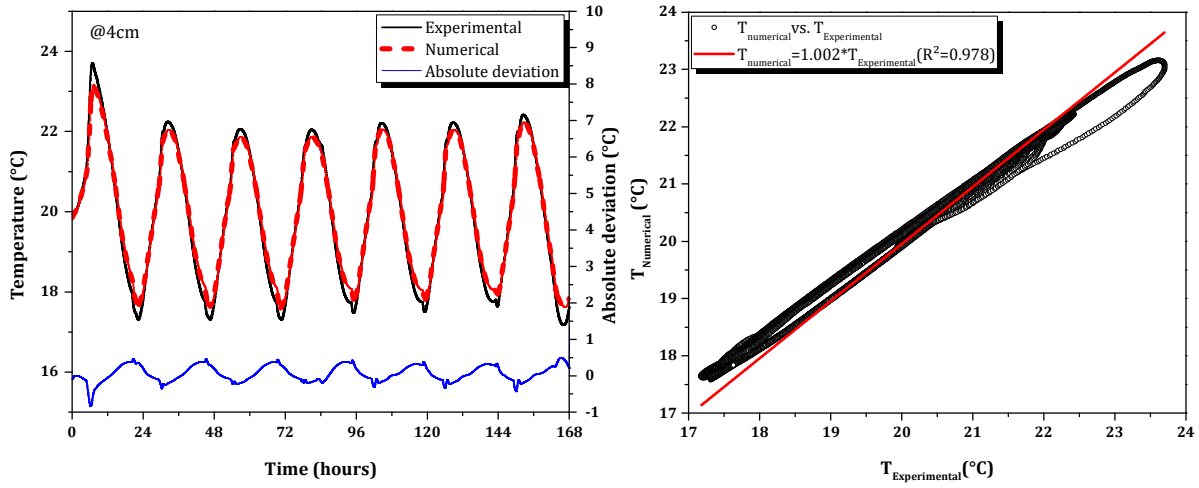

557

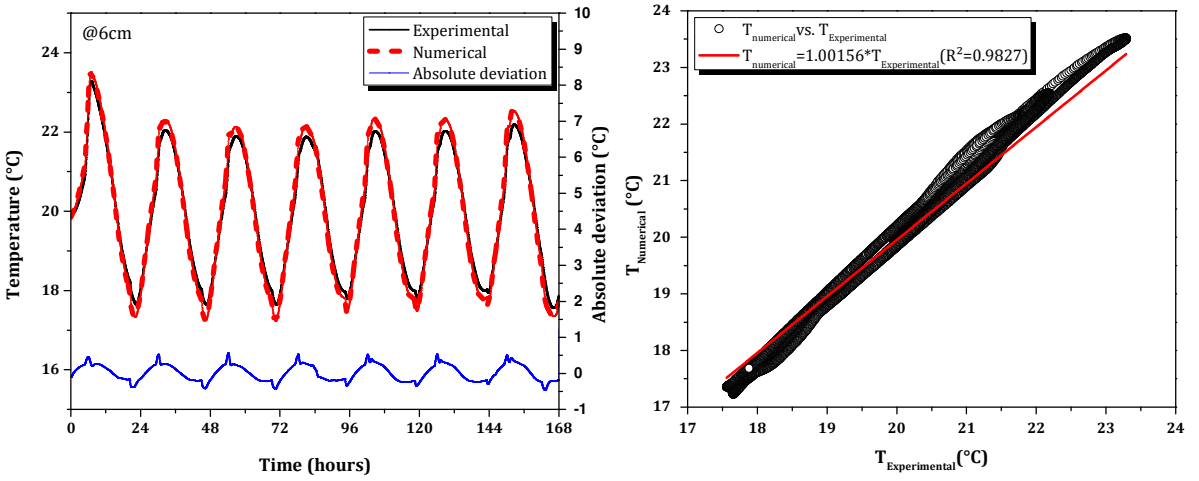

558

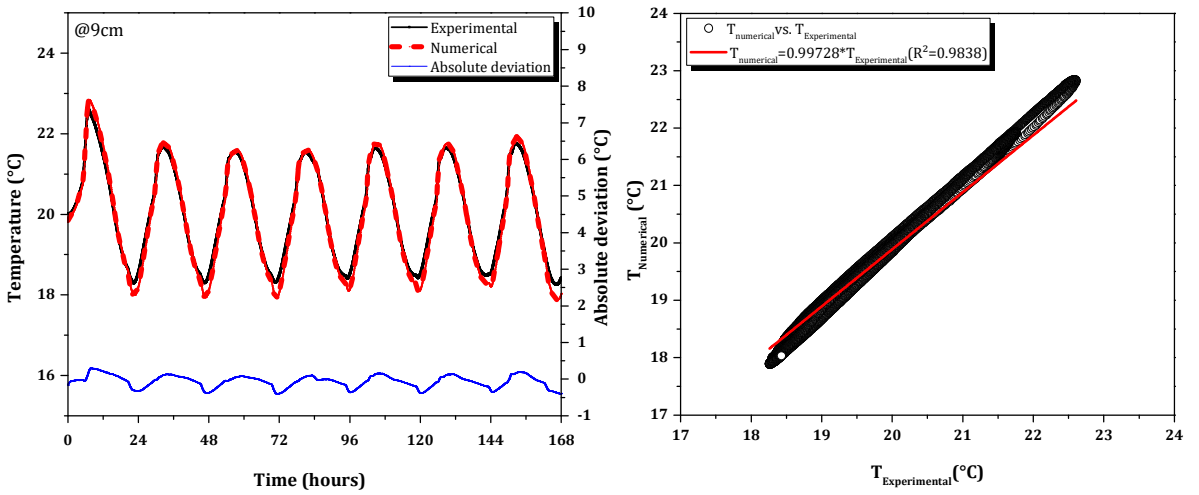

559

560 Fig. 16: Temperature evolution at 4, 6 and 9 cm.

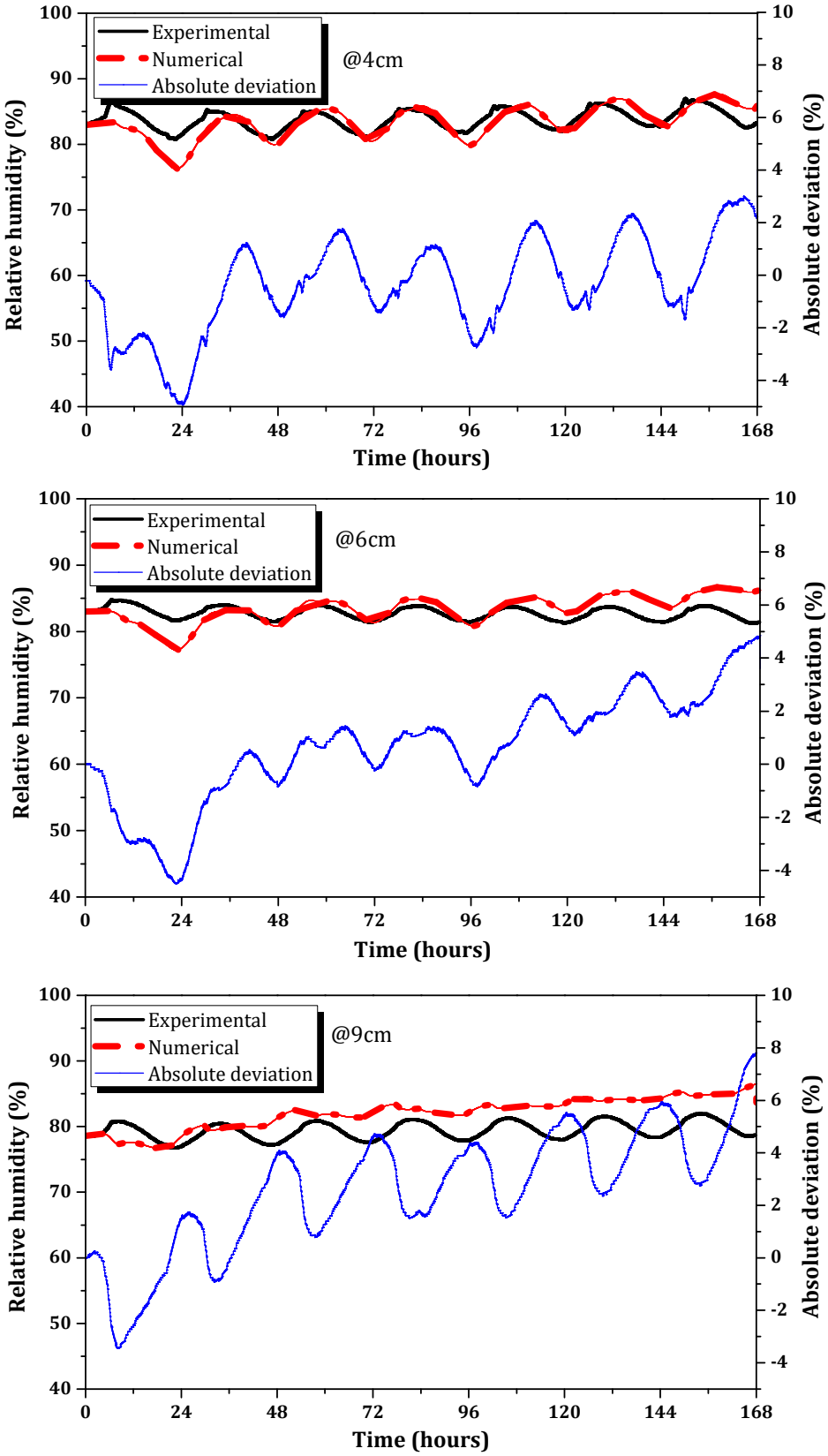

561

562 Fig. 17: Relative humidity evolution at 4, 6 and 9 cm.

In addition, the conducted heat flux measurements were performed on the external and internal borders, as shown in Fig. 18. The results vary between 100 and -40 W/m² at the external border and between 10 and -5 W/m² at the internal border. These values are in agreement with the experimental results obtained from a building scale measurement campaign [36]. The simulated heat flux is in good agreement with the measured flux with R^2 = 0.8964 and 0.7884 for the external/internal border, respectively. Indeed, a good correlation between our experimental observation and the results of the numerical simulation can be seen. However, the simulated flux at the external and internal borders is overestimated by 7% and underestimated by 0.15% respectively, compared with the values measured experimentally. This discrepancy, as mentioned before, can be attributed in part to the fact that the sensor is impermeable to mass transfer. Finally, the ME and RMSE shown in Table 4 of the thermal flux is about 6.71 – 7.79 and 3.07 – 3.64 W.m-2 at the external/internal border, respectively. These values are tolerable and within the margin of accuracy of the sensors used (See Table 1).

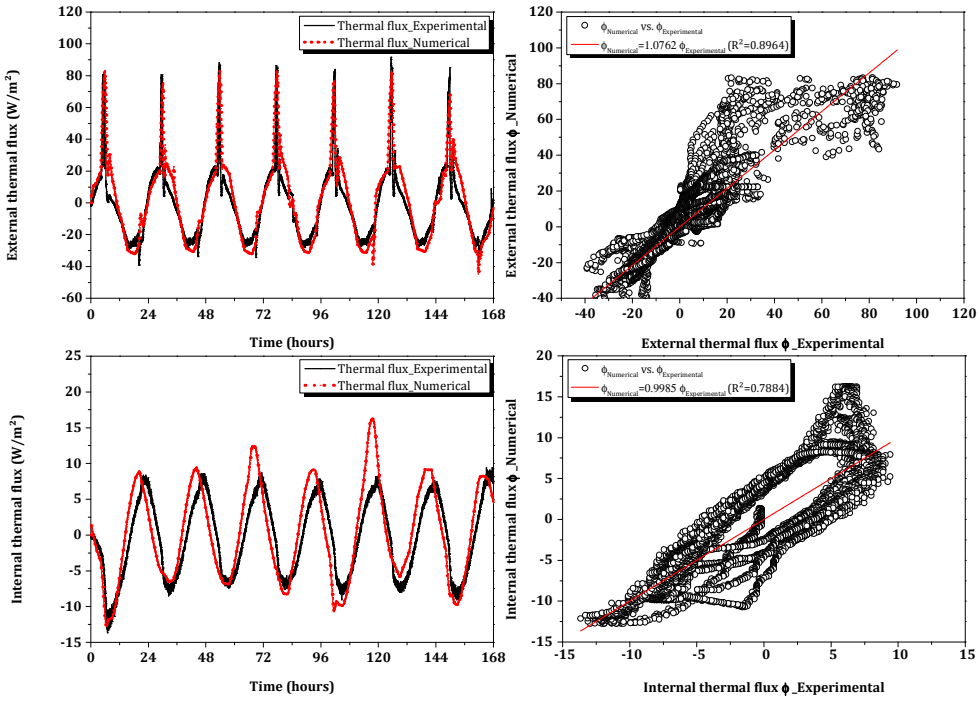

Fig. 18: Comparison of the conducted heat flux of the model prediction with the experimentally measured heat flux at the external and internal borders.

Table 04: MEs and RMSEs between experimental and numerical results.

		x=0	x=4cm	x=6cm	x=9cm	x=11cm
T [°C]	ME	-	0.18	0.20	0.14	-
	RMSE	-	0.23	0.23	0.18	-
RH [%]	ME	-	1.44	1.70	3.02	-
	RMSE	-	1.81	2.12	3.47	-
J_q [W.m^2]	ME	6.71	-	-	-	3.07
	RMSE	7.79	-	-	-	3.64

4.3 Comparison between Test 1 and 2

In order to identify the effect of solar radiation and rainfall on the hygrothermal transfer. A comparison between the both tests was conducted in term of simulated mass flow received in the wall as shown in Figs. 19 and 20. The mass flow at the external borders varies with the same shape as the external loads in T and RH for both tests. It can be seen that the mass flow is larger by 3.33 times in Test 2 than in Test 1 with significant peaks, due to the wetting by liquid water from a rainfall period which the quantity is measured and reported in Fig. 15 of about 280 $g.m^{-2}.h^{-1}$. Nevertheless, the solar radiation also contributes to the drying of the wall. Moreover, and during solar radiation, a high heat flux of about $820W.m^{-2}$ is applied to the external border (see Fig. 15). This evaporates the rainwater stored and trapped in the wall. In general, the mass flux at the external border varies between -1e-3 – 1.5e-3 $kg.m^{-2}.s^{-1}$ and -5e-3 – 5e-3 $kg.m^{-2}.s^{-1}$ for Test 1 and Test 2, respectively. As for the mass flow at the internal border, the value fluctuates between about -3e-4 – 3e-4 $kg.m^{-2}.s^{-1}$ and -4e-5 – 4.5e-5 $kg.m^{-2}.s^{-1}$ for Test 1 and Test 2 respectively. This is due to the fact that the water storage-destorage takes place mainly on the outer side where the dynamic water flow happens.

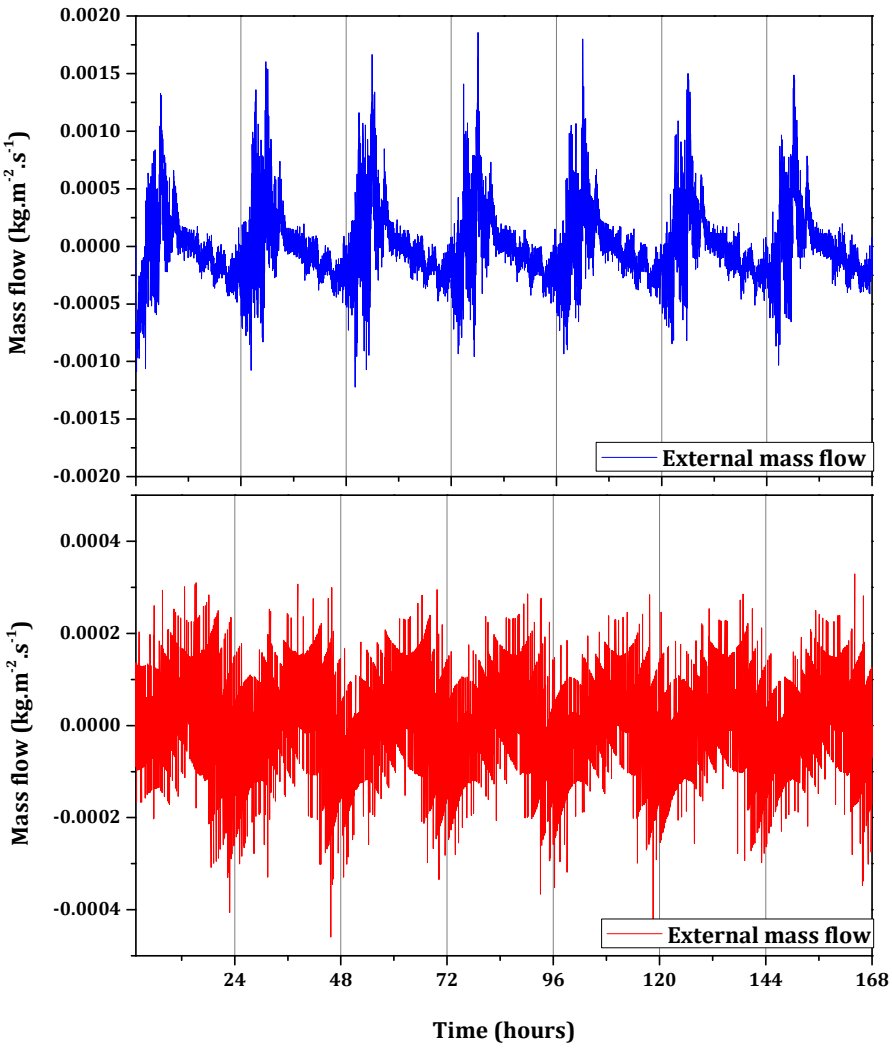

Fig. 19 : Mass flow evolution at the external/internal border-Test 1.

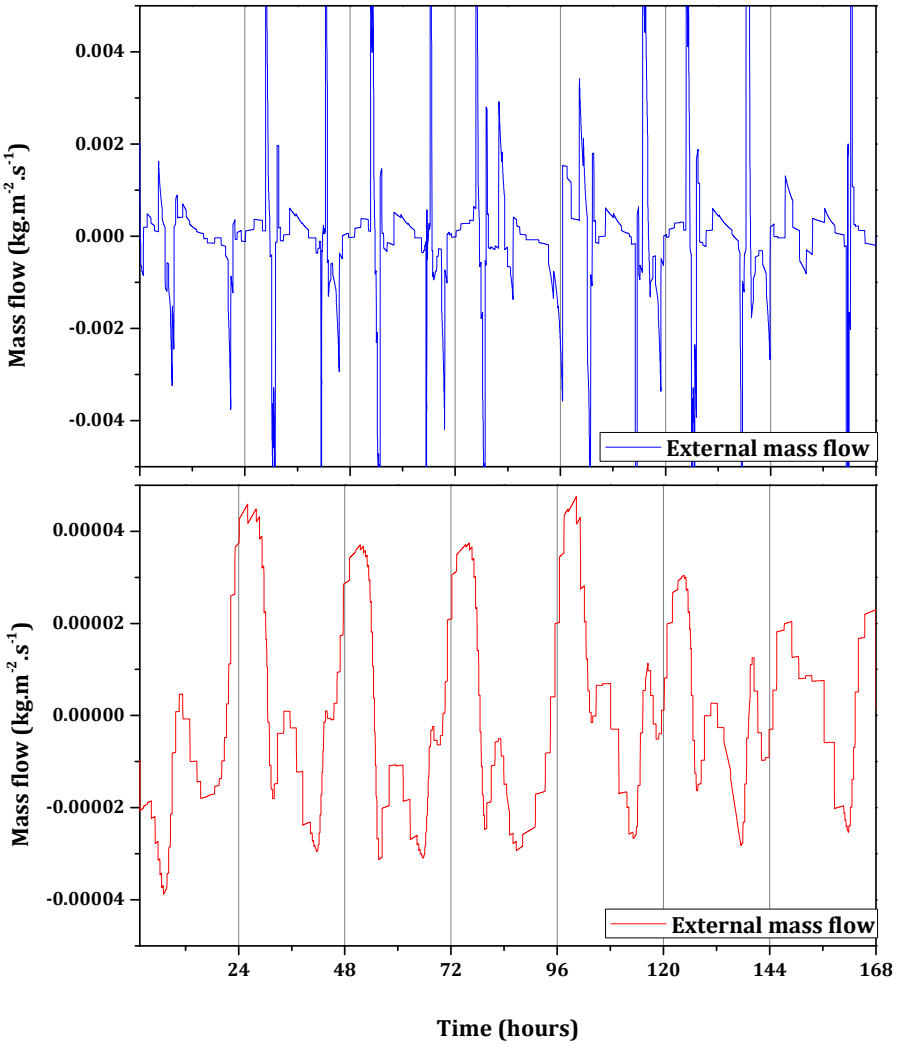

Fig. 20: Mass flow evolution at the external/internal border-Test 2.

4.4 Chemical composition analysis

In this section, chemical composition analysis by ion chromatography (IC) of the rainwater before and after the application of 7 rainfall sequences is measured using an 883 Basic Ion Chromatograph Plus from Metrohm®. This analysis allows us to identify and quantify perfectly the chemical elements present in the solution. In addition, the number of chemical analyses is limited to the initial and final ones due to the fact that the adopted rainfall system is a closed water circuit and it is installed inside the chamber. This allows the temperature of the rainwater to have the same temperature as the chamber environment. In order not to influence this temperature and the climatic conditions applied to the external border during the opening and closing of the compartment, it was required to analyse the water just at the beginning and at the end of the test. Fig. 21 presents a dissolution of the elements of sodium, potassium, magnesium, nitrates and a large quantity of calcium and sulphates. These chemical species are leached from the wall made of the studied eco-concrete, which change its microstructure and chemical composition altering its chemical resistance [67]. The high pH of concrete wich protect the steel reinforcements from corrosion and attacks by aggressive agents is lowered affecting the

durability of the concrete. In fact, the van der Waals force between the mortar and coarse aggregate on the wall surface is reduced under the effect of rain erosion, which causes microcracks in the transition zone of the interface. With increasing rain erosion time, the microcracks become progressively larger, and the small pores on the concrete surface gradually deteriorate into large pores [68]. However, the chemical analysis shows an increase in the amount of chloride present in the water used during the rainfall. The chloride content in the wall decreases with application of the rainfall period [69].

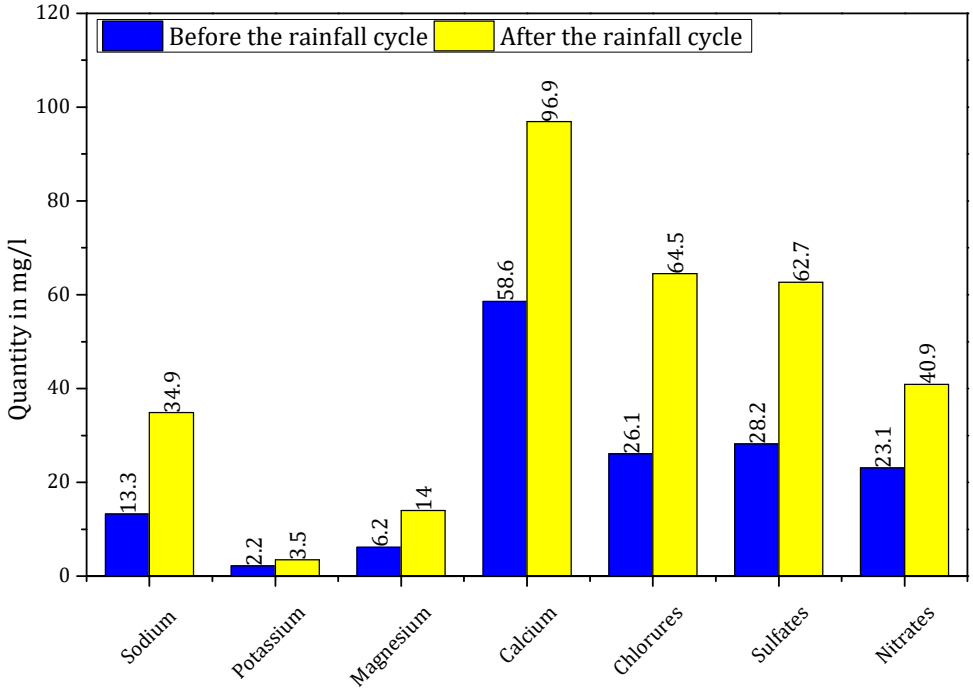

Fig. 21: Chemical composition of rainwater before and after rainfall cycle.

5 Sensitivity analysis

In this section, the objective is to evaluate the effect of several parameters on the response of the hygrothermal model. Indeed, the effect of the variations of several material parameters on the numerical results was evaluated by considering ±20% of variations of these inputs compared to their reference values. This part of the study deals with the influence of input material parameters on the model's results. Significant errors are usually present on these parameters, due to measurement uncertainties at the material scale, or to the use of these parameters at higher scales as mentioned earlier (wall and building scales). This latter reason (transition from the material to the wall scale) may be responsible for much higher uncertainties on input values, because manufacturing a sample of large dimensions can probably generate a wider range of uncertainties on the materials properties and on the homogeneity of the system [70]. In the present work, to evaluate the influence of a varying parameter on the resulting T and Pv profiles, the relative sensitivity index is calculated as follows [71]:

$$S\,(\%) = \frac{Y_{p+\delta p} - Y_{p-\delta p}}{2Y_p} \times 100 \quad (21)$$

Where Y is the solution of the model (T or P_v), Y_p is the reference solution obtained when no parameter is changed (all parameters are set to their reference values), p indicates the variable parameter and δp the variation range. This relative sensitivity index is calculated considering 20% of variation of input parameters with respect to their reference valuesnging from 20% [72]. Low percentages represent errors that may occur at the material scale, while high percentages are related to errors at higher scales due to the accumulation of small errors. The sensitivity of the present model has been investigated with respect to the following parameters: density, heat capacity, thermal conductivity, water vapor/liquid permeability and sorption isotherm that is used to define the water content w in the hygrothermal model under the thermodynamic equilibrium hypothesis.

In this step, each parameter was changed separately considering 20% of variation (δP : − 20% and +20% of the reference value), while the other parameters were kept constant at their initial values. The different configurations of this sensitivity analysis are summarized in Figs. 22 and 23. Calculations were carried out for the two tests previously described in section 4 (test under sinusoidal effects without solar radiation nor rainfall and test with solar radiation and rainfall). Indeed, 13 different simulations were run for each scenario, representing a total of 26 simulations for the overall study. Figs. 22 and 23 show the T and Pv sensitivity evolutions at different depths (4, 6 and 9cm) for Test 1 and Test 2, respectively. Which were calculated considering variations of ±20% on each parameter with respect to the reference value. It can be observed that the maximum sensitivity values are reached at the same time as the external temperature signal changes and not exceed 0.2% for Test 1 and 0.6% for Test 2, whether it is for thermal conductivity, heat capacity and density, and the change effect of mass transfer parameter on the heat transfer is very negligible. From the mass transfer point of view, the impact of density variation and sorption isotherms is very dominant and may reach 1.5% for both tests, compared to vapor permeabilities which has almost no effect. Whereas the thermal conductivity, liquid permeability and specific heat variation allows a change in the mass transfer sensitivity results with 0.25% and 0.75 % for Test 1 and Test 2, respectively.

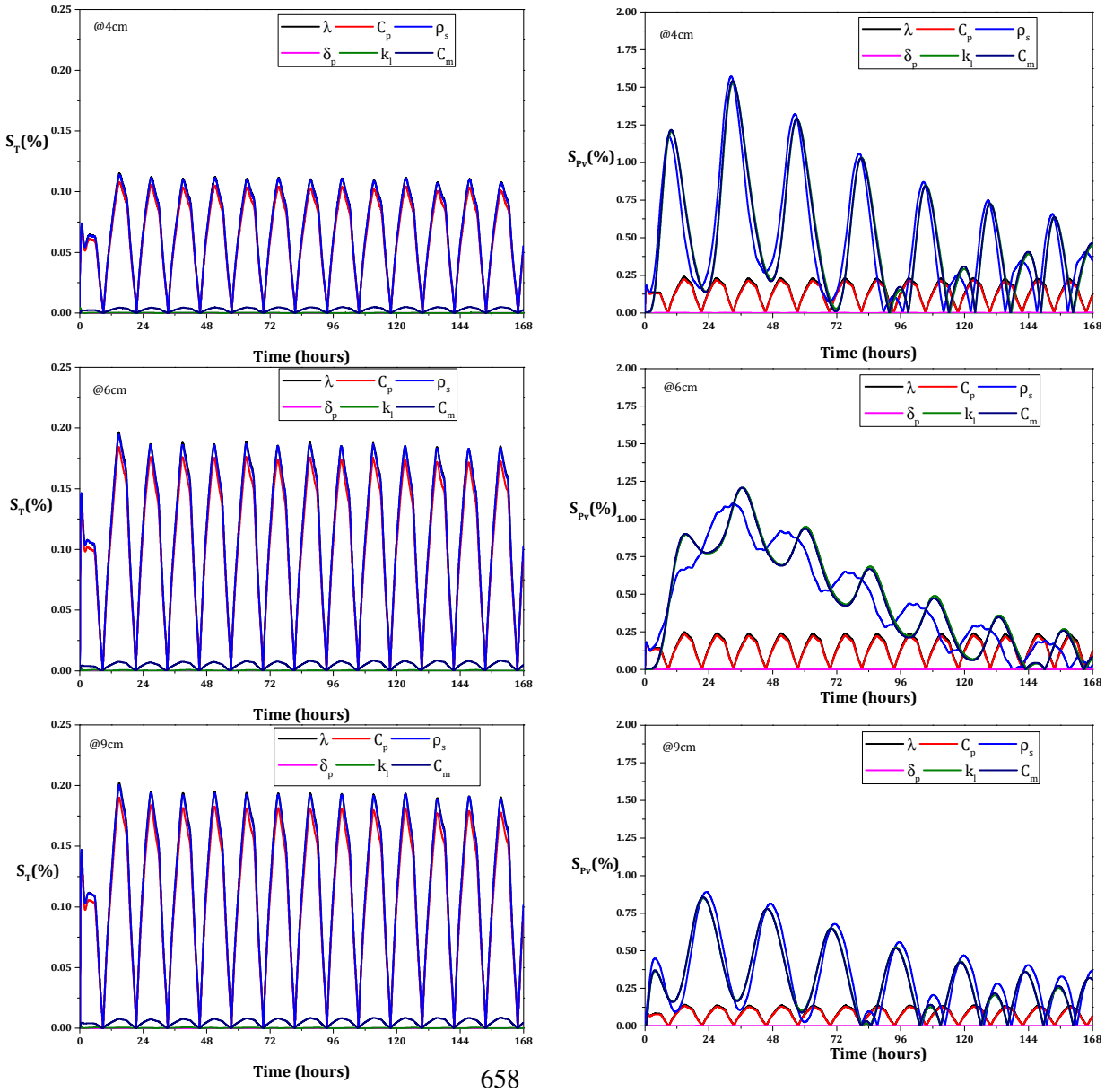

658

659 Fig. 22: T and Pv sensitivities evolution to a ±20% change of parameters related to reference value
660 and at different depths of the studied wall: 4 , 6 and 9cm - Test 1.

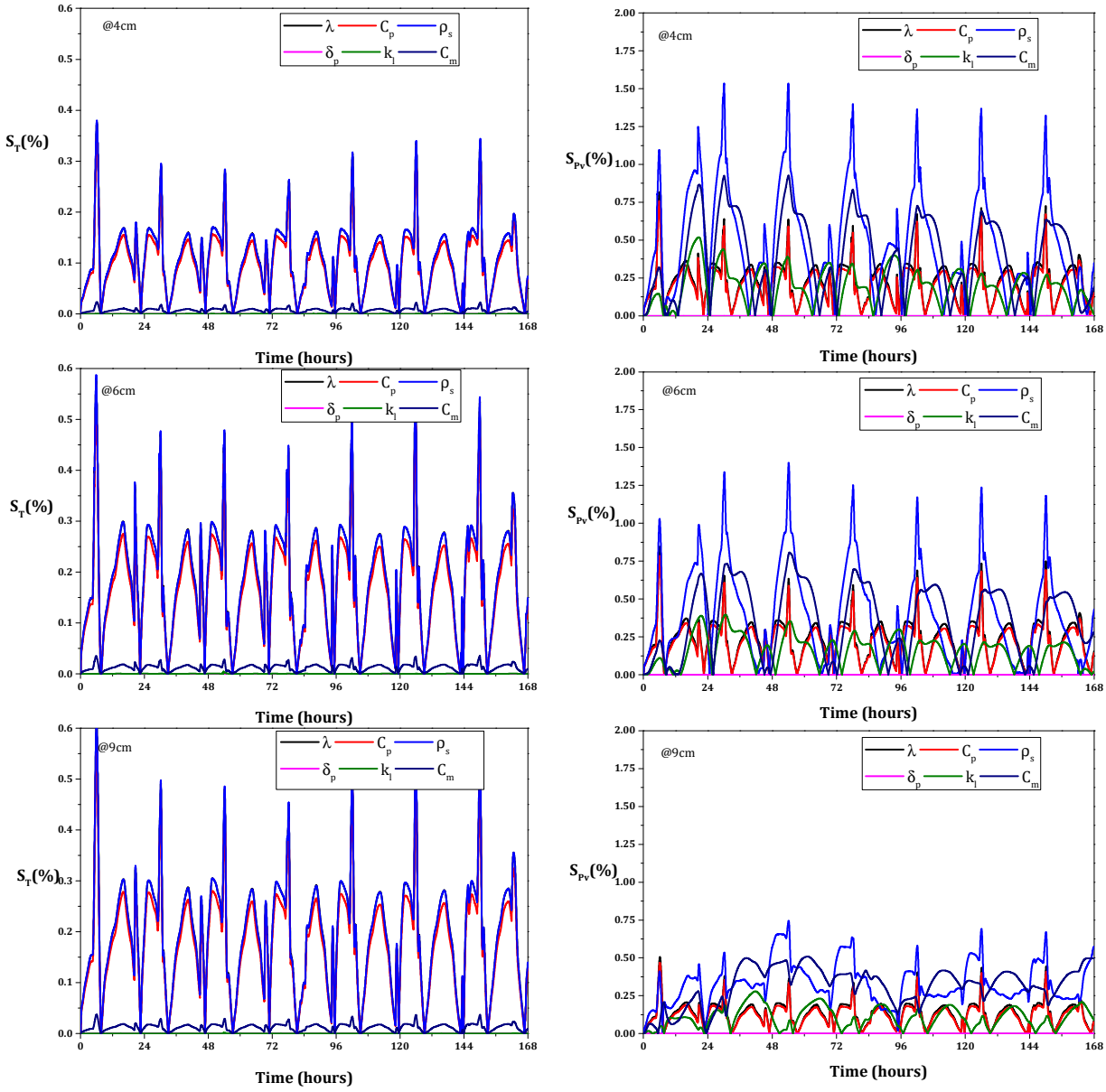

Fig. 23: T and Pv sensitivities evolution to a ±20% change of parameters related to reference value and at different depths of the studied wall: 4 , 6 and 9cm - Test 2.

6 Conclusion

This article presents an experimental and numerical study of the hygrothermal behavior of a wall building made of new eco-concrete based on glass powder as a partial replacement of cement. The wall is subjected to drying/wetting by dynamic climatic conditions such as solar radiations and rainfall which are rarely studied in the literature. The coupled heat and mass transfer model takes into account the effect of solar radiations and rainfall at the boundaries. The hygrothermal envelope model was validated by comparison against experimental results. The experimental data have been generated via the developed experimental bench. This apparatus allows the simulation of different climatic

672 conditions, such as variations of temperature, humidity, rainfall and solar radiation. The simulation of
673 the hygrothermal behavior of the eco-concrete wall highlights that the hygrothermal model is required
674 for better prediction the relative humidity and temperature response through the wall as well as the
675 heat flux at the external/internal borders.

676 For the first test without solar radiation nor rainfall, the absolute deviation does not exceed 0.3 °C for
677 the temperature and 2% for relative humidity. For thermal flux, a very good correlation between our
678 experimental observation and the results of the numerical simulation is found. It is underestimated by
679 2.3% and overestimated by 10% for the internal and external borders respectively, compared with the
680 values measured experimentally.

681 In the case of second test with solar radiation and rainfall, the largest errors are recorded at the time of
682 the maximum or minimum value of temperature in the outdoor chamber, but these always remain
683 within the error range of the sensors used, and gradually as we get further away from the external
684 border. Concerning the thermal flux, the simulated heat flux is in good agreement with the measured
685 flux. The simulated flux is overestimated by 7% and underestimated by 0.15% at the external and
686 internal borders respectively, compared with the values measured experimentally.

687 The proposed model has a good agreement with the experimental results, and the ME and RMSE of
688 the temperature, relative humidity and thermal flux are within the acceptable levels. As for the mass
689 flow at the external border, it varies between -1e-3 – 1.5e-3 $kg.m^{-2}.s^{-1}$ and -5e-3 – 5e-3 $kg.m^{-2}.s^{-1}$ for
690 Test 1 and Test 2, respectively. At the internal border, the value fluctuates between about -3e-4 – 3e-4
691 $kg.m^{-2}.s^{-1}$ and -4e-5 – 4.5e-5 $kg.m^{-2}.s^{-1}$ for Test 1 and Test 2, respectively. To summarize, the mass
692 flow is larger by 3.33 times in Test 2 than in Test 1 with significant peaks and the solar radiation
693 contributes to the drying of the wall by evaporating the rainwater stored and trapped in the wall.

694 The chemical analysis of the water used to simulate rainfall before and after rain sequences show a
695 release of chemical species from the studied wall. These chemical species are responsible for the
696 chemical resistance and the hight pH of an eco-concrete. In addition, the analysis showed a release of
697 an amount of chloride responsible for the corrosion of the reinforced concrete steels.

698 A sensitivity analysis was also carried out and it showed that envelope hygrothermal performance is
699 very sensitive to thermal conductivity, heat capacity and density for the thermal transfer and to
700 sorption isotherm curve, density and less important for the thermal conductivity, heat capacity and
701 water liquid permeability for the mass transfer and even negligible for the water vapor permeability.

702 In over all, this data can be used in the energy performance study of environmentally friendly
703 buildings. Indeed, further development of the hygrothermal transfer model in porous media, taking

into account the effect of radiation on rainfall and vice versa, the using flux-type boundary conditions and the sustainability study of wall studied is the objective of future studies.

Acknowledgement

The Nouvelle Aquitaine Region and the European Union support the project < CPER-FEDER Bâtiment durable Axis 2 MADUR Project: High-performance building materials with low environmental impact, sustainable and resilient > within the framework of the "Operational Program FEDER/FSE 2015-2020" and the Energy saving certificate program of the Ministry of Ecological and Solidarity Transition "SmartReno support" 2019–2021.

References

[1] S. Roels, Experimental analysis of moisture buffering. Final Report IEA-ECBCS Annex 41 'Whole Building Heat, Air, Moisture Response'. Leuven: ACCO, (2008).

[2] F. Tariku, K. Kumaran, P. Fazio, Erratum to: Determination of indoor humidity profile using a whole-building hygrothermal model, Build. Simul. 4 (2011) 277–277. https://doi.org/10.1007/s12273-011-0033-8.

[3] H. Ge, X. Yang, P. Fazio, J. Rao, Influence of moisture load profiles on moisture buffering potential and moisture residuals of three groups of hygroscopic materials, Build. Environ. 81 (2014) 162–171. https://doi.org/10.1016/j.buildenv.2014.06.021.

[4] L.K. Holm A, Moisture buffering effect—experimental investigations and validation, in: Proc. Build. X Conf. Therm. Perform. Exter. Envel. Whole Build. Clear. Bach, FL, USA., 2007.

[5] K. Abahri, R. Belarbi, N.O. B, N. Issaadi, M. Ferroukhi, Total Pressure Gradient Incidence on Hygrothermal Transfer in Highly Porous Building Materials, Adv. Mater. Res. 772 (2013) 124–129. https://doi.org/10.4028/www.scientific.net/AMR.772.124.

[6] M.Y. Ferroukhi, R. Djedjig, K. Limam, R. Belarbi, Hygrothermal behavior modeling of the hygroscopic envelopes of buildings: A dynamic co-simulation approach, Build. Simul. 9 (2016) 501–512. https://doi.org/10.1007/s12273-016-0292-5.

[7] M.Y. Ferroukhi, R. Belarbi, K. Limam, W. Bosschaerts, Impact of Coupled Heat and Moisture Transfer, Therm. Sci. 21 (2017) 1359–1368.

[8] Z. Slimani, A. Trabelsi, J. Virgone, R.Z. Freire, Study of the hygrothermal behavior of wood fiber insulation subjected to non-isothermal loading, Appl. Sci. 9 (2019). https://doi.org/10.3390/app9112359.

[9] A. Trabelsi, Z. Slimani, J. Virgone, Response surface analysis of the dimensionless heat and mass transfer parameters of Medium Density Fiberboard, Int. J. Heat Mass Transf. 127 (2018) 623–630. https://doi.org/10.1016/j.ijheatmasstransfer.2018.05.145.

[10] T. Alioua, B. Agoudjil, N. Chennouf, A. Boudenne, K. Benzarti, Investigation on heat and moisture transfer in bio-based building wall with consideration of the hysteresis effect, Build. Environ. 163 (2019) 106333. https://doi.org/10.1016/j.buildenv.2019.106333.

[11] T. Alioua, B. Agoudjil, A. Boudenne, K. Benzarti, Sensitivity analysis of transient heat and moisture transfer in a bio-based date palm concrete wall, Build. Environ. 202 (2021) 108019. https://doi.org/10.1016/j.buildenv.2021.108019.

[12] A. V. Luikov, Heat and mass transfer in capillary-porous bodies, Pergamon Press. Oxford 1 Édn. (1966).

[13] A. Trabelsi, R. Belarbi, K. Abahri, M. Qin, Assessment of temperature gradient effects on moisture transfer through thermogradient coefficient, Build. Simul. 5 (2012) 107–115. https://doi.org/10.1007/s12273-012-0063-x.

[14] M. Qin, R. Belarbi, Development of an analytical method for simultaneous heat and moisture transfer in building materials utilizing transfer function method, J. Mater. Civ. Eng. 17 (2005) 492–497. https://doi.org/10.1061/(ASCE)0899-1561(2005)17:5(492).

[15] M.Y. Ferroukhi, R. Belarbi, K. Limam, Effect of Hygrothermal Transfer on Multilayer Walls Behavior, Assessment of Condensation Risk, Adv. Mater. Res. 1051 (2014) 647–655. https://doi.org/10.4028/www.scientific.net/AMR.1051.647.

[16] H.S.L.C. Hens, Heat, Air and Moisture Transfer In Highly Insulated Building Envelopes (HAMTIE), IEA ECBCS Annex. 24 (2002) 21.

[17] J. Grunewald, Diffusiver und konvektiver Stoff- und Energie- transport in kapillarporösen Baustoffen, Diss. TU Dresden. (1996) 220.

[18] A. Janssens, Reliable control of interstitial condensation in lightweight roof systems, Leuven, 1997.

[19] A. TenWolde, Moisture Transfer Through Materials and Systems in Buildings, in: Water Vap. Transm. Through Build. Mater. Syst. Mech. Meas., ASTM International, 100 Barr Harbor Drive, PO Box C700, West Conshohocken, PA 19428-2959, n.d.: pp. 11-11–8. https://doi.org/10.1520/STP22953S.

[20] S.L.C.H. Hens, Building Physics - Heat, Air and Moisture 3e Fundamentals and Engineering Methods with Examples and Exercises, Wilhelm Ernst & Sohn, Berlin, Germany, 2017. https://doi.org/10.1002/9783433608548.

[21] M. Rahim, O. Douzane, A.D. Tran Le, G. Promis, T. Langlet, Experimental investigation of hygrothermal behavior of two bio-based building envelopes, Energy Build. 139 (2017) 608–615. https://doi.org/10.1016/j.enbuild.2017.01.058.

[22] P.A. Moradias, P.D. Silva, J.P. Castro-Gomes, M.V. Salazar, L. Pires, Experimental study on hygrothermal behaviour of retrofit solutions applied to old building walls, Constr. Build. Mater. 35 (2012) 864–873. https://doi.org/10.1016/j.conbuildmat.2012.04.138.

[23] M.Y. Ferroukhi, K. Abahri, R. Belarbi, K. Limam, A. Nouviaire, Experimental validation of coupled heat, air and moisture transfer modeling in multilayer building components, Heat Mass Transf. Und Stoffuebertragung. 52 (2016) 2257–2269. https://doi.org/10.1007/s00231-015-1740-y.

[24] R. Tejeda-Vázquez, E.V. Macias-Melo, I. Hernández-Pérez, K.M. Aguilar-Castro, J. Serrano-Arellano, Empirical model of hygrothermal behavior of masonry wall under different climatic conditions using a hot box, Energy Build. 249 (2021) 111209. https://doi.org/10.1016/j.enbuild.2021.111209.

[25] P.M. Congedo, C. Baglivo, D. D'Agostino, G. Quarta, P. Di Gloria, Rising damp in building stones: Numerical and experimental comparison in lecce stone and carparo under controlled microclimatic conditions, Constr. Build. Mater. 296 (2021) 123713. https://doi.org/10.1016/j.conbuildmat.2021.123713.

[26] M.-A. Hamdaoui, M.-H. Benzaama, Y. El Mendili, D. Chateigner, A review on physical and data-driven modeling of buildings hygrothermal behavior: Models, approaches and simulation tools, Energy Build. 251 (2021) 111343. https://doi.org/10.1016/j.enbuild.2021.111343.

[27] H.M. Künzel, Simultaneous Heat and Moisture Transport in Building Components One and

two dimensional calculation using simple parameter, Fraunhofer IRB Verlag. (1995).

[28] S. Rouchier, M. Woloszyn, G. Foray, J.-J. Roux, Influence of concrete fracture on the rain infiltration and thermal performance of building facades, Int. J. Heat Mass Transf. 61 (2013) 340–352. https://doi.org/10.1016/j.ijheatmasstransfer.2013.02.013.

[29] H. Janssen, Wind-driven rain as a boundary condition for HAM simulations: Analysis of simplified modelling approaches, Build. Environ. 42 (2007) 1555–1567. https://doi.org/10.1016/j.buildenv.2006.10.001.

[30] H. Janssen, Conservative modelling of the moisture and heat transfer in building components under atmospheric excitation, Int. J. Heat Mass Transf. 50 (2007) 1128–1140. https://doi.org/10.1016/j.ijheatmasstransfer.2006.06.048.

[31] T. Ihara, B.P. Jelle, T. Gao, A. Gustavsen, Aerogel granule aging driven by moisture and solar radiation, Energy Build. 103 (2015) 238–248. https://doi.org/10.1016/j.enbuild.2015.06.017.

[32] B. Blocken, J. Carmeliet, A simplified numerical model for rainwater runoff on building facades: Possibilities and limitations, Build. Environ. 53 (2012) 59–73. https://doi.org/10.1016/j.buildenv.2012.01.010.

[33] B. Blocken, D. Derome, J. Carmeliet, Rainwater runoff from building facades: A review, Build. Environ. 60 (2013) 339–361. https://doi.org/10.1016/j.buildenv.2012.10.008.

[34] American Society of Heating, Refrigerating and Air-Conditioning Engineers (ASHRAE), 2013. ANSI/ASHRAE Standard 55-2013: Thermal Environmental Conditions for Human Occupancy. American Society of Heating, Refrigerating and Air-Conditioning Engineers, Inc., (2013).

[35] S.E. Ouldboukhitine, R. Belarbi, R. Djedjig, Characterization of green roof components: Measurements of thermal and hydrological properties, Build. Environ. 56 (2012) 78–85. https://doi.org/10.1016/j.buildenv.2012.02.024.

[36] R. Djedjig, R. Belarbi, E. Bozonnet, Experimental study of green walls impacts on buildings in summer and winter under an oceanic climate, Energy Build. 150 (2017) 403–411. https://doi.org/10.1016/j.enbuild.2017.06.032.

[37] R. Djedjig, E. Bozonnet, R. Belarbi, Modeling green wall interactions with street canyons for building energy simulation in urban context, Urban Clim. 16 (2016) 75–85. https://doi.org/10.1016/j.uclim.2015.12.003.

[38] M. Nascimento, J. Gonçalves Pareira, G. Alves Lira, V.D.S.F. Dantas, André A. Nobrega, Hygrothermal simulation : Use for service life prediction and maintenance of façade, Eco-Architecture. 183 (2019) 139–149. https://doi.org/doi:10.2495/ARC180131.

[39] L.A. De Mello, L.M. Moura, N. Mendes, International Journal of Thermal Sciences A model for predicting heat , air and moisture transfer through fibrous materials, Int. J. Therm. Sci. 145 (2019) 106036. https://doi.org/10.1016/j.ijthermalsci.2019.106036.

[40] R.A. Pescaru, L. Dumitrescu, I. Baran, C.M. Grădinaru, Comparative Analysis of Hygrothermal Behaviour of the Exterior Walls in Transient Regime, IOP Conf. Ser. Mater. Sci. Eng. 586 (2019). https://doi.org/10.1088/1757-899X/586/1/012011.

[41] F. Tariku, E. Iffa, Empirical model for cavity ventilation and hygrothermal performance assessment of wood frame wall systems: Experimental study, Build. Environ. 157 (2019) 112–126. https://doi.org/10.1016/j.buildenv.2019.04.020.

[42] H. Rafidiarison, R. Rémond, E. Mougel, Dataset for validating 1-D heat and mass transfer

models within building walls with hygroscopic materials, Build. Environ. 89 (2015) 356–368. https://doi.org/10.1016/j.buildenv.2015.03.008.

[43] S.K. Asphaug, B. Time, T. Kvande, Hygrothermal simulations of thermally insulated basement envelopes - Importance of boundary conditions below grade, Build. Environ. 199 (2021) 107920. https://doi.org/10.1016/j.buildenv.2021.107920.

[44] French Government, 'Exigences réglementaires pour la construction des batiments'. Ministère de la Transition écologique et solidaire, 2019. http://www. ecologique-solidaire.gouv.fr/exigences-reglementaires-construction-des-batiments., (n.d.).

[45] F. Boukhelf, Proposition d'une nouvelle formulation mathématique pour l'analyse du comportement thermo hydro mécanique des structures fonctionnellement graduées, Thèse de Doctorat de La Rochelle université, 2020.

[46] J. Fourier, Théorie analytique de la chaleur, 1822 , Édouard Leroy, « Sur l'intégration des équations de la chaleur », 14 (1897) 379–465.

[47] J. Berger, T. Busser, S. Reddy, G.S. Dulikravich, Evaluation of the reliability of a heat and mass transfer model in hygroscopic material, Int. J. Heat Mass Transf. 142 (2019) 118258. https://doi.org/10.1016/j.ijheatmasstransfer.2019.06.014.

[48] X. Liu, Y. Chen, H. Ge, P. Fazio, G. Chen, Numerical investigation for thermal performance of exterior walls of residential buildings with moisture transfer in hot summer and cold winter zone of China, Energy Build. 93 (2015) 259–268. https://doi.org/10.1016/j.enbuild.2015.02.016.

[49] B. Remki, K. Abahri, M. Tahlaiti, R. Belarbi, Hygrothermal transfer in wood drying under the atmospheric pressure gradient, Int. J. Therm. Sci. 57 (2012) 135–141. https://doi.org/10.1016/j.ijthermalsci.2012.02.005.

[50] ©COMSOL Introduction to application builder. U.S. Patents, (2016).

[51] H. Janssen, J. Carmeliet, Hygrothermal simulation of masonry under atmospheric excitation, Proc. 3rd Int. Build. Phys. Conf. - Res. Build. Phys. Build. Eng. (2006) 77–82.

[52] B. Stute, V. Krupp, E. von Lieres, Performance of iterative equation solvers for mass transfer problems in three-dimensional sphere packings in COMSOL, Simul. Model. Pract. Theory. 33 (2013) 115–131. https://doi.org/10.1016/j.simpat.2012.10.004.

[53] M. Beneš, P. Mayer, Coupled model of hygro-thermal behavior of concrete during fire, J. Comput. Appl. Math. 218 (2008) 12–20. https://doi.org/10.1016/j.cam.2007.04.031.

[54] F. Boukhelf, R. Cherif, A. Trabelsi, R. Belarbi, M. Bachir Bouiadjra, On the hygrothermal behavior of concrete containing glass powder and silica fume, J. Clean. Prod. (2021) 128647. https://doi.org/10.1016/j.jclepro.2021.128647.

[55] EN 12664, Performance thermique des matériaux et produits pour le bâtiment - Détermination de la résistance thermique par la méthode de la plaque chaude gardée et la méthode fluxmétrique - Produits secs et humides de moyenne et basse résistance thermiqu, 2001.

[56] EN 12667, Performance thermique des matériaux et produits pour le bâtiment - Détermination de la résistance thermique par la méthode de la plaque chaude gardée et la méthode fluxmétrique - Produits de haute et moyenne résistance thermique,», 2001.

[57] NF EN 821-3, Céramiques techniques avancées - Céramiques monolithiques - Propriétés thermophysiques - Partie 3 : détermination de la chaleur spécifique, Juin 2005, 2005.

[58] D. Choqueuse, A. Chomard, P. Chauchot, How to provide relevant data for the prediction of long term behavior of insulation materials under hot/wet conditions?, Offshore Technology Conference (OTC 16503), Houston, Texas (U.S.A.), 2004., (n.d.).

[59] ISO 12571, Performance hygrothermique des matériaux et produits pour le bâtiment, Détermination des propriétés de sorption hygroscopique, 2000.

[60] S. Furmaniak, A.P. Terzyk, P.A. Gauden, The general mechanism of water sorption on foodstuffs - importance of the multitemperature fitting of data and the hierarchy of models, J. Food Eng. (2007) 528–535.

[61] H. Yoshino, T. Mitamura, K. Hasegawa, Moisture buffering and effect of ventilation rate and volume rate of hygrothermal materials in a single room under steady state exterior conditions, Build. Environ. 44 (2009) 1418–1425. https://doi.org/10.1016/j.buildenv.2008.09.007.

[62] H. M. Rafidiarison, Etudes expérimentales des transferts de masse et de chaleur dans les parois des constructions en bois, en vue de leur modélisation. Applications aux économies d'énergie et au confort dans l'habitat, Thèse de doctorat, RP2E - Ecole Doctorale Sciences et Ingénierie des Ressources, Procédés, Produits, Environnement, France., 2012.

[63] L.F. Hidalgo, M.N. Candido, K. Nishioka, J.T. Freire, G.N.A. Vieira, Natural and forced air convection operation in a direct solar dryer assisted by photovoltaic module for drying of green onion, Sol. Energy. 220 (2021) 24–34. https://doi.org/10.1016/j.solener.2021.02.061.

[64] A. Chavan, V. Vitankar, A. Mujumdar, B. Thorat, Natural convection and direct type (NCDT) solar dryers: a review, Dry. Technol. (2020) 1–22. https://doi.org/10.1080/07373937.2020.1753065.

[65] M. Maaroufi, F. Bennai, R. Belarbi, K. Abahri, Experimental and numerical highlighting of water vapor sorption hysteresis in the coupled heat and moisture transfers, J. Build. Eng. 40 (2021) 102321. https://doi.org/10.1016/j.jobe.2021.102321.

[66] R. Rodrigues, S. Gaboreau, J. Gance, I. Ignatiadis, S. Betelu, Reinforced concrete structures: A review of corrosion mechanisms and advances in electrical methods for corrosion monitoring, Constr. Build. Mater. 269 (2021) 121240. https://doi.org/10.1016/j.conbuildmat.2020.121240.

[67] S.-C. Han, Y. Jo, J.-I. Yun, Chemical degradation of fly ash blended concrete with the seasonal variation of rainwater in a radioactive waste repository: A thermodynamic modeling approach, Cem. Concr. Res. 141 (2021) 106326. https://doi.org/10.1016/j.cemconres.2020.106326.

[68] C. Carde, R. François, Modelling the loss of strength and porosity increase due to the leaching of cement pastes, Cem. Concr. Compos. 21 (1999) 181–188. https://doi.org/10.1016/S0958-9465(98)00046-8.

[69] H. Jin, J. Liu, Z. Jiang, H. Zhou, J. Liu, Influence of the rainfall intensity on the chloride ion distribution in concrete with different levels of initial water saturation, Constr. Build. Mater. 281 (2021) 122561. https://doi.org/10.1016/j.conbuildmat.2021.122561.

[70] Y. Aït Oumeziane, S. Moissette, M. Bart, F. Collet, S. Pretot, C. Lanos, Influence of hysteresis on the transient hygrothermal response of a hemp concrete wall, J. Build. Perform. Simul. 10 (2017) 256–271. https://doi.org/10.1080/19401493.2016.1216166.

[71] A. Boudenne, L. Ibos, Y. Candau, Analysis of uncertainties in thermophysical parameters of materials obtained from a periodic method, Meas. Sci. Technol. 17 (2006) 1870–1876. https://doi.org/10.1088/0957-0233/17/7/027.

[72] M. Bart, S. Moissette, Y. Ait Oumeziane, C. Lanos, Transient hygrothermal modelling of coated hemp-concrete walls, Eur. J. Environ. Civ. Eng. 18 (2014) 927–944.

https://doi.org/10.1080/19648189.2014.911122.